

NASA TECHNICAL
MEMORANDUM

NASA TM X-53743

1968

NASA TM X-53743

INSTRUMENTATION RESEARCH FOR GROUND TESTING AT MSFC

N 68-30625

N 68-30629

FACILITY FORM 602

(ACCESSION NUMBER)

(THRU)

(PAGES)

(CODE)

(NASA CR OR TMX OR AD NUMBER)

(CATEGORY)

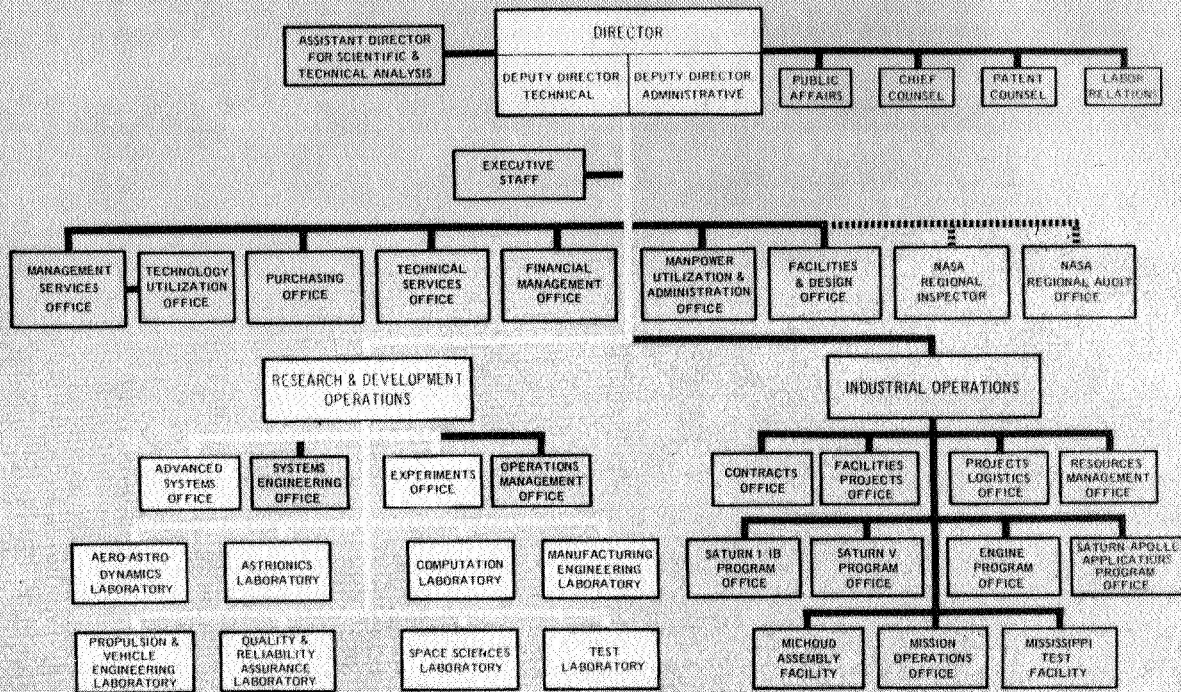
RESEARCH ACHIEVEMENTS REVIEW

VOLUME II

REPORT NO. 12

RESEARCH AND DEVELOPMENT OPERATIONS
GEORGE C. MARSHALL SPACE FLIGHT CENTER
HUNTSVILLE, ALABAMA

GEORGE C. MARSHALL SPACE FLIGHT CENTER



RESEARCH ACHIEVEMENTS REVIEWS COVER THE FOLLOWING FIELDS OF RESEARCH

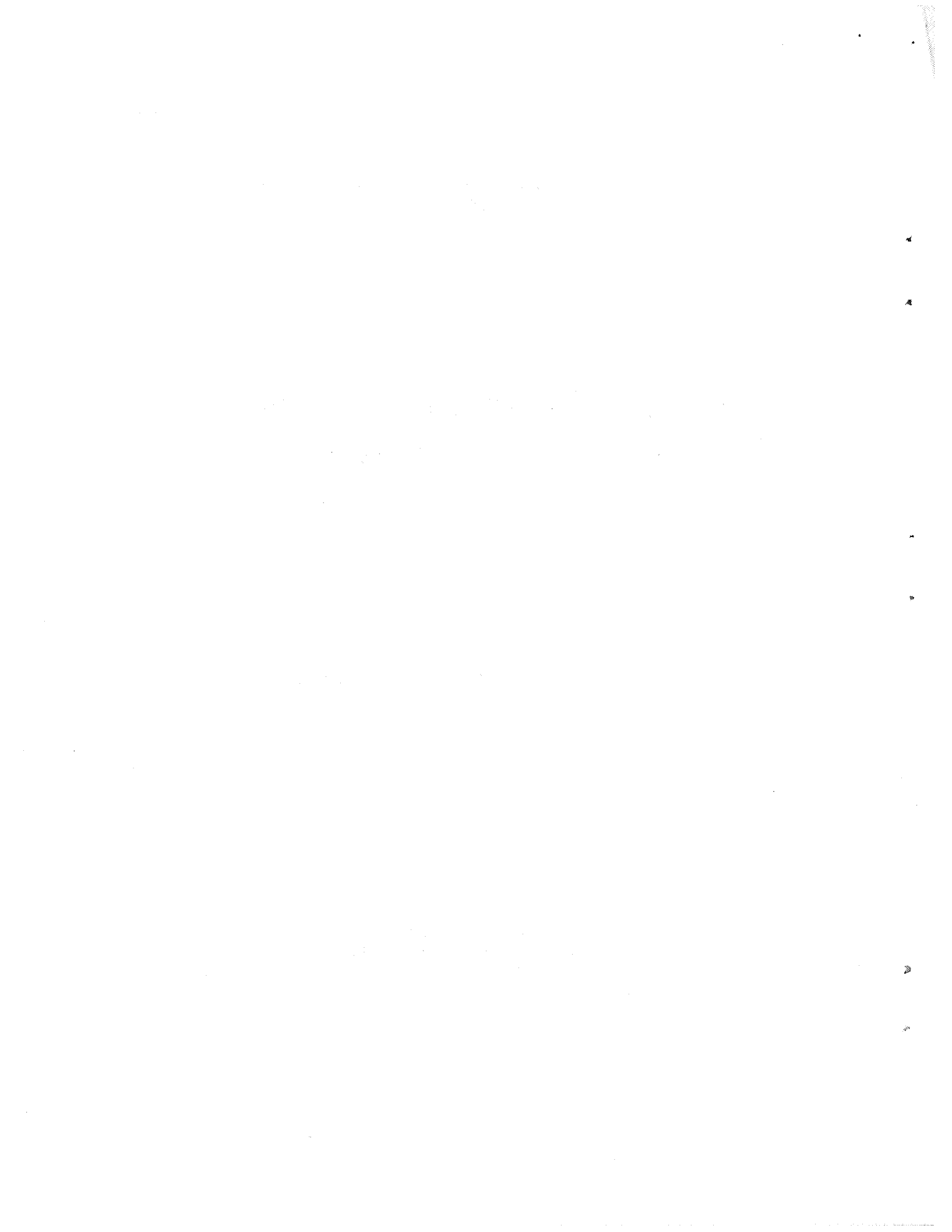
- Radiation Physics
- Thermophysics
- Chemical Propulsion
- Cryogenic Technology
- Electronics
- Control Systems
- Materials
- Manufacturing
- Ground Testing
- Quality Assurance and Checkout
- Terrestrial and Space Environment
- Aerodynamics
- Instrumentation
- Power Systems
- Guidance Concepts
- Astrodynamics
- Advanced Tracking Systems
- Communication Systems
- Structures
- Mathematics and Computation
- Advanced Propulsion
- Lunar and Meteoroid Physics

NATIONAL AERONAUTICS AND SPACE ADMINISTRATION
WASHINGTON, D. C.

RESEARCH ACHIEVEMENTS REVIEW
VOLUME II REPORT NO.12

INSTRUMENTATION RESEARCH FOR GROUND TESTING AT MSFC

RESEARCH AND DEVELOPMENT OPERATIONS
GEORGE C. MARSHALL SPACE FLIGHT CENTER
HUNTSVILLE, ALABAMA



PRECEDING PAGE BLANK NOT FILMED.

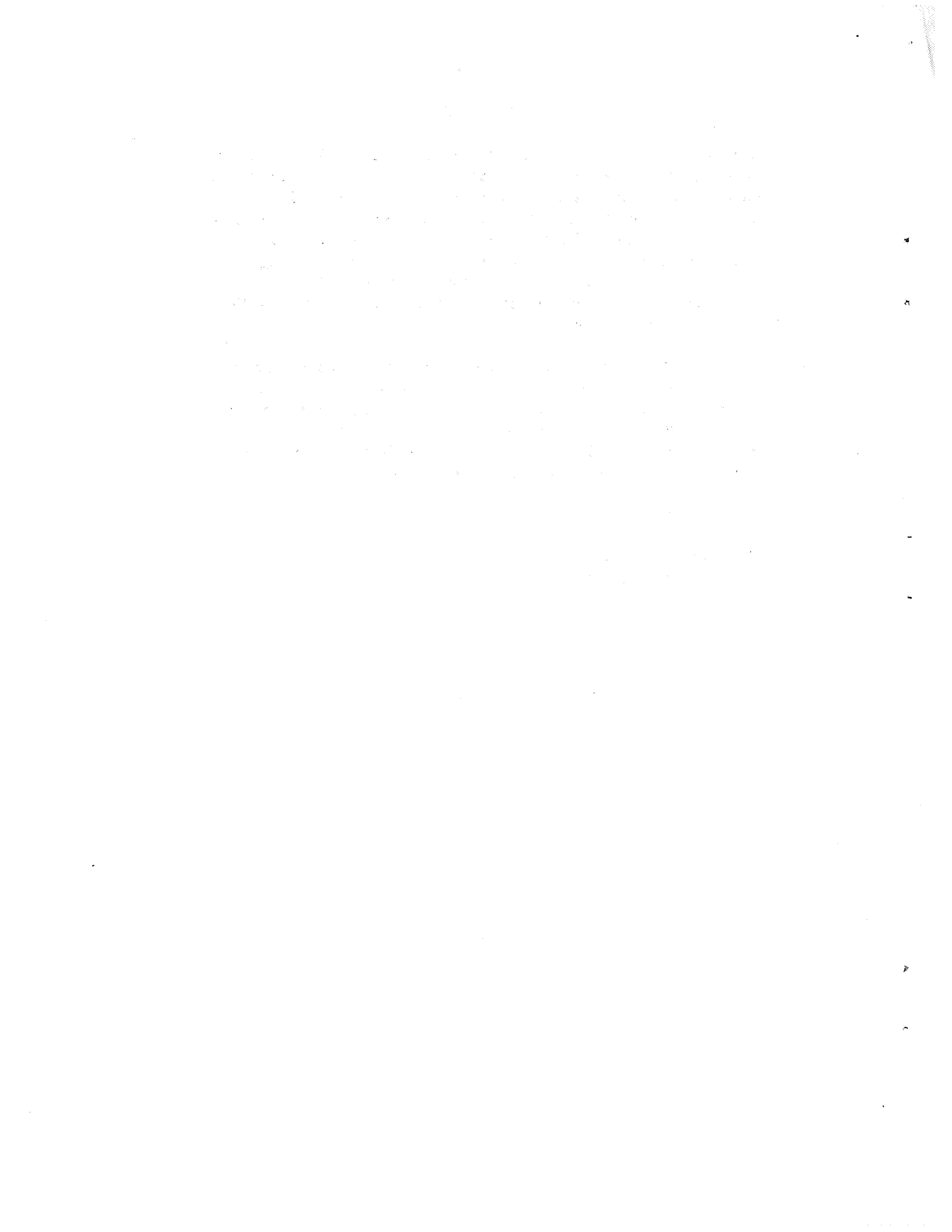
PREFACE

In February 1965, Dr. Ernst Stuhlinger, Director, Research Projects Laboratory (now Space Sciences Laboratory), initiated a series of Research Achievements Reviews which set forth those achievements accomplished by the laboratories of the Marshall Space Flight Center. Each review covered one or two fields of research in a form readily usable by specialists, systems engineers and program managers. The review of February 24, 1966, completed this series. Each review has been documented in the "Research Achievements Review Series."

In March 1966, a second series of Research Achievements Reviews was initiated. This second series has emphasized research areas of greatest concentration of effort, of most rapid progress, or of most pertinent interest and published as "Research Achievements Review Reports, Volume II." Volume II will cover the reviews extending from March 1966 through February 1968.

The papers in this report were presented January 25, 1968

William G. Johnson
Director, Experiments Office



CONTENTS ...

**INTRODUCTION TO INSTRUMENTATION RESEARCH FOR
GROUND TESTING AT MSFC**

by Albert E. Schuler **Page** 1

✓ **HYDROGEN SLUSH DENSITY INSTRUMENTATION**

by Alvin M. Payne

SUMMARY	3
HYDROGEN SLUSH DENSITY REFERENCE SYSTEM	3
NUCLEAR RADIATION ATTENUATION TRANSFER STANDARD	7
INTERNAL POINT DENSITOMETER	8
REFERENCES	9

LIST OF ILLUSTRATIONS

Figure	Title	
1.	Cryostat and Container Filled with Triple-Point Liquid Hydrogen.	3
2.	Hydrogen Slush in Container; Cryostat Filled with Triple-Point Liquid	4
3.	Graph Showing Results of Error Analysis	5
4.	Details of Cryostat for Determination of Hydrogen Slush Density	6
5.	450-Liter Hydrogen Slush Generator with NRA Densitometer	8
6.	NRA Densitometer Results	8
7.	ORTEC Slush Hydrogen Densitometer	9

✓ **PRESSURE TRANSDUCERS FOR ENVIRONMENTAL EXTREMES**

by Harlan S. Harman

SUMMARY	11
HIGH TEMPERATURE, HIGH FREQUENCY RESPONSE PRESSURE TRANSDUCER	11
Typical Specifications	12
Signal Transmission	13
Rocket Motor Test Arrangement	13
Inner Column of Transducer	14
Frequency Response	14
Installation and Compensation of the Strain Gage Bridge	15

CONTENTS (Continued) ...

	Page
CRYOGENIC PRESSURE TRANSDUCER	15
REFERENCES	17

LIST OF ILLUSTRATIONS

Figure	Title	
1.	Conceptual Design	12
2.	Sectional View of Transpirationally Cooled Pressure Transducer	12
3.	Rocket Motor Test Arrangement	14
4.	Inner Column and Assembled Transducer	14
5.	Balco Wire Compared with N-Type GaSb Gage Resistance	16
6.	GaSb Transducer	16
7.	Gage Factor Change vs Temperature	16
8.	Cryogenic Pressure Transducer — Zero and Sensitivity Shift with Temperature	16
9.	Typical Transducer Elements	17
10.	Disassembled Cryogenic Pressure Transducer	17
11.	Completed Transducers	17
12.	Typical Performance Curve (Response of Transducer Zero Output to Step Change in Temperature)	17

✓ THE USE OF THE MÖSSBAUER EFFECT AND LASER INTERFEROMETRY TO DETERMINE EXTREMELY SMALL AMPLITUDES FOR VIBRATION MEASUREMENTS AND CALIBRATIONS

by Helmut G. Lackner

SUMMARY	19
INTRODUCTION	19
MOSSBAUER EFFECT	19
LASER INTERFEROMETRY	27

LIST OF ILLUSTRATIONS

Figure	Title	Page
1.	Mössbauer Line and Emission and Absorption Line	20
2.	Principle of Mössbauer Apparatus and Doppler-Shifted Gamma Line	20
3.	Calibration Spectrum for Stainless Steel Alloy 310 Enriched	21
4.	Quadrupole Splitting	21
5.	Nuclear Zeeman Effect	21
6.	Diagram of the Partial Resonance Case Transfer Function	22
7.	Electronic Sampling	22
8.	Amplitude Measurements of a Piezoelectric Shaker	23
9.	Comparison of Experimental and Calculated Peak Displacements of a Piezoelectric Transducer	23
10.	Useful Range of Partial Resonance Case	24
11.	Multiple Point Calibration Technique Transfer Function	24
12.	Loudspeaker Calibration by Resonance Absorption Line Position	25
13.	Useful Range of the Multiple Point Calibration Technique	25
14.	Resonance Case Absorption Curves	26
15.	Source Mounted on Loudspeaker	26
16.	Source Mounted on PZT-5 Crystal	26
17.	Useful Range of the Resonance Case	26
18.	Mössbauer Effect Vibration Calibrator	27
19.	Block Diagram of the Laser Interferometry System	29
20.	Output of the Fundamental, of the First Harmonic, Their Ratio, and of the Monitoring Accelerometer Versus Shaker Driving Voltage	29
21.	Output of the Fundamental, of the First Harmonic, and Their Ratio Versus Shaker Driving Voltage	30
22.	Multiple Beam Reflection Interferometer	31

✓ PARACTOR, A NEW TOOL FOR ACCURATE DC AMPLIFICATION AND DIGITAL DATA TRANSMISSION

by Thomas L. Greenwood

INTRODUCTION	33
PARACTOR RESEARCH AND DEVELOPMENT	33
MULTICHANNEL DIGITAL DATA ACQUISITION SYSTEM	34
Design of 120 Channel System	34
Development of Comparator Circuit	34
Description of the System	36
Additional Applications	37
CONCLUSIONS	38

LIST OF ILLUSTRATIONS

Figure	Title	
1.	Pulsed Paractor	33
2.	Paractor Magnetic Circuit	33
3.	Initial Input Configuration	35
4.	Improved Circuit	35
5.	Final Configuration	35
6.	Arrangement of Components	36
7.	System Block Diagram	36
8.	Precision Amplifier Using Paractor	37
9.	Precision DC Amplifier	37

INTRODUCTION TO INSTRUMENTATION RESEARCH FOR GROUND TESTING AT MSFC

By

Albert E. Schuler

The research and development activities of the Instrument Development Branch in the Test Instrumentation and Control Division comprise inhouse and contracted basic and applied research to provide instruments and measuring or calibration systems required for the various activities of the Test Laboratory. In addition to the four papers selected for this review, total success in some programs and partial progress in a few other programs will be discussed very briefly in the following paragraphs.

A hydrogen gas detector was developed under a completed research contract with Beckman Instruments. In this electrochemical or polarographic instrument the hydrogen diffuses through a polystyrene diaphragm into a catalytic cell where hydrogen molecules ionize and generate a current proportional to the partial pressure of hydrogen in the gas mixture. This hydrogen detector was used successfully at the S-II stand of the Mississippi Test Facility.

Spacecraft, Inc., developed an analytical system to determine how much liquid nitrogen mixes with the liquid oxygen when the LO_2 tank is pressurized with gaseous nitrogen. This instrument utilizes the electric susceptibility difference between the two liquids. Calibration and test stand applications demonstrated the accuracy and reliability of this instrument. Later a dielectric circuit was developed for optional plug-in to determine the water vapor content of the gas.

In an inhouse research program an instrument was developed for measurement of pulse flow on attitude motors. Studies and research measurements led to a contract for modification of a flowmeter prover system originally developed by the Flow Technology Corporation under the sponsorship of Edwards Air Force Base. The main purpose of this positive displacement meter was to provide in-line spot checks of turbine flowmeter calibration factors. The meter uses a precision piston-cylinder assembly within a fluid bypass chamber. To make a measurement, the piston is released to obstruct the entrance to the bypass chamber; this forces the liquid and piston through the cylinder. The piston passes two or more Hall-effect switches that are used to determine the time for displacing an accurately known volume. In our modified version the motion of the piston is measured by

an optical encoder that transmits 52.8 pulses/cm³ (200,000 pulses/gal or about 900 pulses/in.³). After successful laboratory tests the instrumentation is now being prepared for use on the test stand. This prover system is very accurate and provides an entirely new concept of flowmeter calibration for measuring moderate quantities, which could be desirable in many applications that include the S-IVB Orbital Workshop and other long range missions.

In another successfully completed project a 25.4-cm (10-in.) diameter liquid hydrogen densitometer for the S-IVB suction line was developed and delivered to MSFC by Industrial Nucleonics Corporation. This meter uses nuclear radiation attenuation, and the tests so far indicate very good results.

A completed study contract with Industrial Nucleonics Corporation was requested to determine the feasibility of using nuclear methods for hydrogen mass flow measurement. As a result, Industrial Nucleonics Corporation proposed to develop a nuclear mass flowmeter, but their study did not indicate sufficient evidence for success of their proposal. Therefore a contract was not awarded. Instead, a nuclear mass flowmeter was designed to operate by injecting beta particles at one end of the flow tube and using capacitive detection of their velocity and density at the other end of the flow tube. Presently, Oak Ridge National Laboratory will build this meter for \$10,000 for delivery in June 1968.

In another research project, Trans-Sonics, Inc., used the nuclear resonance technique to develop a digital thermometer for measuring cryogenic temperatures in the range of 3 to 100°K with an accuracy of ± 5 millidegrees. In this technique, a material such as chromium tribromide or potassium chloride is placed in the field of a high frequency oscillator. The nuclei of the material will start to resonate, reorient themselves, and absorb energy from the oscillator when the frequency of the oscillator reaches the nuclear resonance frequency of the material. This frequency is a function of temperature, and thus the calibration factor depends only on the chemical structure of the sample and not on its dimensions, which is a great advantage. A laboratory model of this nuclear resonance thermometer has been built

and tested. The soundness of the principle has been established, and an extension of the contract is planned to build a workable field instrument, including a servo system for regulating the oscillator frequency to the nuclear resonance frequency at the respective temperature.

A contract with Engineering Physics Corporation is for the development of a mass flowmeter with a separate density or quality indication needed for slush hydrogen research and testing. This instrument uses the electromagnetic induction principle with a high frequency electromagnet to measure the velocity of the nonconductive liquid, and the Clausius-Masotti relation between density and dielectric constant is used for density measurement. There was a problem to join the dielectric nonmagnetic spool piece for the electromagnet with the stainless steel flow line. This problem seems to be solved by using a stainless steel adapter to press the fiber glass against the stainless steel. The breadboard setup of the electronics for

the flowmeter is in working condition, and the design of the meter will soon be completed for manufacturing the flowmeter.

For test and calibration of this and other mass flow and quality meters for weighing volumes of liquid and slush hydrogen, a flow stand with advanced features was designed in an inhouse research project. A stand pipe is used for draining LH_2 without affecting the weighing. A triple tank arrangement permits having a very light tank for weighing the hydrogen, since the open tank for weighing liquids has the same pressure inside and outside. A weighing system with calibration weights and remotely programmed weight application permits calibration checks at any time. In another version the weighing system might be used only as a comparator. During the test, weights are added that have the same mass as the mass of liquid hydrogen taken out of the tank. The tank and the weight system are being manufactured by Inca Corporation and are due at MSFC in June 1968.

HYDROGEN SLUSH DENSITY INSTRUMENTATION

By

Alvin M. Payne

SUMMARY

The transition of liquid hydrogen to slush hydrogen, which is the reducing of a mass of hydrogen to a more compact form, will help to achieve the prolonged space storage of fuel that is essential for long-term missions. Thus slush hydrogen will increase the cryogenic storage capabilities of hydrogen fueled space vehicles. Meaningful testing and analysis of test results to determine the mass of the slush hydrogen can only be accomplished when accurate and reliable measurements of slush quality or density are available. This paper describes the development of an accurate slush density reference system and two different transfer standards for making reliable field measurements of the mass of slush hydrogen after calibration with the reference system.

HYDROGEN SLUSH DENSITY REFERENCE SYSTEM

Figures 1 and 2 illustrate the principle of the slush hydrogen reference system. A cryostat is nearly full of triple-point liquid hydrogen and a lightweight container is completely submerged in this liquid hydrogen, while hanging on a weighing system on top of the cryostat. First the weight container is filled with triple-point liquid hydrogen (Fig. 1) and the scale of the weight-system is made to read zero. Then solid hydrogen is introduced into the weight tank and the weight system indicates the weight of the solid introduced minus the weight of the triple-point liquid displaced (Fig. 2). The quantity, now measured by the weighing system, is the apparent or buoyed weight of the solid, and it can be used in the following equation to compute the solid mass fraction (quality) of the hydrogen slush contained in the weight container:

$$\rho Vg - \rho_l Vg = M_b g$$

$$\rho = \frac{M_b}{V} + \rho_l \quad (1)$$

where

- ρ = density of the hydrogen slush
- ρ_l = density of triple point hydrogen
- V = Volume of the weight container
- M_b = Apparent mass of the buoyed solid
- g = local acceleration of gravity

One of the most accurate methods of determining density is the application of Archimedes' principle. The density of a solid is determined by weighing it while it is submerged in liquids with known densities. The density of a liquid is determined by submerging and weighing a solid body with a known mass and volume. Slush hydrogen, a mixture of solid and liquid, can be weighed in a lightweight container that is suspended by a weighing system and submerged in triple-point liquid hydrogen.

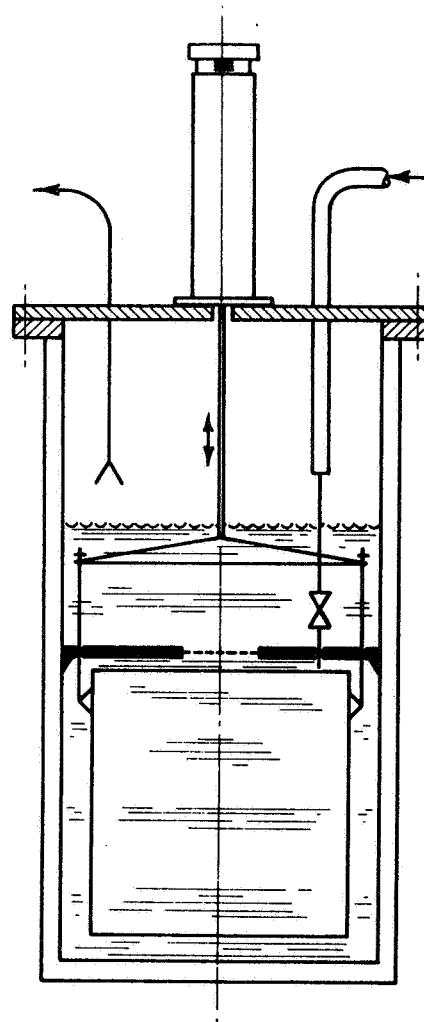


FIGURE 1. CRYOSTAT AND CONTAINER FILLED WITH TRIPLE-POINT LIQUID HYDROGEN

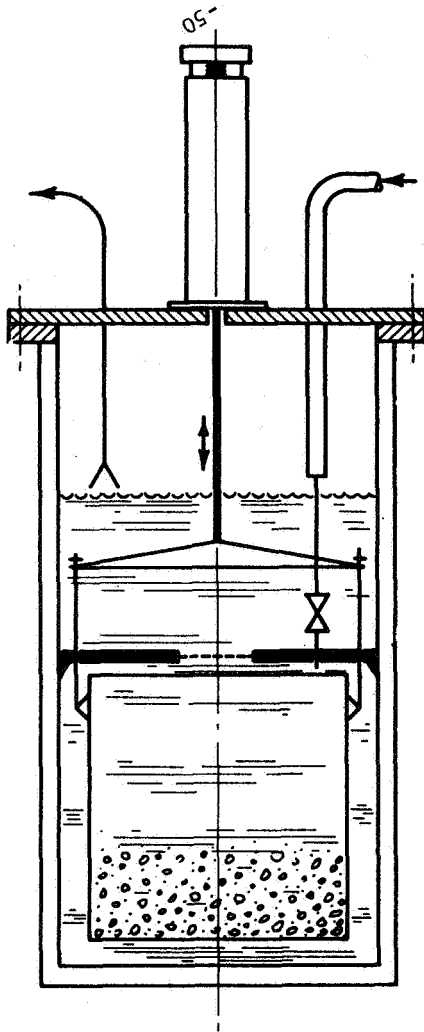


FIGURE 2. HYDROGEN SLUSH IN CONTAINER;
CRYOSTAT FILLED WITH TRIPLE-POINT LIQUID

The Volume, V , is determined with water at ambient temperature, before assembling the reference system. Buoyancy and shrinkage corrections are applied to this value. As a double check the volume, V , is also determined by the difference in weight of the container, filled with triple-point liquid hydrogen, and the weight of the empty container. Hydrogen gas at constant low temperature surrounds the container at both weighings and a buoyancy correction, based on the density of this gas, is applied to the results. The difference in the weight of the hydrogen filled container and the empty container is used to compute the volume of the container as follows:

$$\text{Weight full} - \text{Weight empty} = M_l g = \rho_l Vg$$

$$V = \frac{M_l}{\rho_l}$$

where

M_l = mass of triple point liquid hydrogen

ρ_l = density of triple point liquid hydrogen

Substituting the above quantity for V in equation (1) gives the slush density

$$\rho = \rho_l \left(\frac{M_b}{M_l} + 1 \right) \quad (2)$$

The density of triple-point liquid hydrogen is a physical constant and known from literature [1] to be 77.017 g/l with an uncertainty of $\pm 0.1\%$. M_b and M_l must be determined by weighing. M_l is a constant for the particular reference system and is about 2000 g for the container with a diameter of 28 cm and a depth of 37 cm. The value of M_b will vary from a few grams for a low solid fraction to about 137 g for 60% solid fraction.

An error analysis for the reference system requires some reasonable assumptions of the weight determination. If calibration masses and a suitable method for their application and removal during the experiment are provided, it should be quite easy to determine both M_b and M_l to within $\pm 0.5\%$ of their true values. However, to determine a safe value of the accuracy limits, it is assumed that the inaccuracy in the weighing can be as much as $\pm 2.0\%$.

A general expression for compounding of errors in y , where $y = f(x_1, x_2, \dots, x_n)$

is

$$(dy)^2 = \sum_{i=1}^n \left(\frac{\partial f}{\partial x_i} \right)^2 (dx_i)^2$$

if the components of error, dx , are independently distributed and symmetrical with respect to positive and negative values [2]. Using this rule for equation (2),

$$(d\rho)^2 = \left(\frac{\partial\rho}{\partial\rho_l}\right)^2 (d\rho_l)^2 + \left(\frac{\partial\rho}{\partial M_b}\right)^2 (dM_b)^2 + \left(\frac{\partial\rho}{\partial M_l}\right)^2 (dM_l)^2 \quad (3)$$

typical values for the variables are as follows:

$$M_b = 117 \text{ g (the value for a solid fraction of 0.50)}$$

$$M_l = 2000 \text{ g}$$

$$\rho_l = 77.017 \text{ g/l .}$$

From these values and the assumed fractional errors in weighing, together with the ± 0.1 uncertainty in ρ_l , the following relationship can be made:

$$\frac{dM_b}{M_b} = 0.02, \text{ or } dM_b = 2.34 \text{ g}$$

$$\frac{dM_l}{M_l} = 0.02, \text{ or } dM_l = 40.0 \text{ g}$$

$$\frac{d\rho_l}{\rho_l} = 0.001, \text{ or } d\rho_l = 0.077 \text{ g/l.}$$

The partial derivatives are

$$\frac{\partial\rho}{\partial\rho_l} = \left(\frac{M_b}{M_l} + 1\right) = 1.05856$$

$$\frac{\partial\rho}{\partial M_b} = \frac{\rho_l}{M_l} = 0.03854$$

$$\frac{\partial\rho}{\partial M_l} = \frac{-\rho_l M_b}{M_l^2} = -0.002256 .$$

From equation (3),

$$(d\rho)^2 = 0.00665 + 0.00814 + 0.00818, \text{ or}$$

$$(d\rho)^2 = 0.0230, \text{ and}$$

$$d\rho = \pm 0.15 \text{ g/l .}$$

Note that the three terms which add together to get $(d\rho)^2$ are approximately equal in magnitude even though the uncertainty in the triple-point liquid density (which gives the first term) is $\pm 0.1\%$, whereas the

uncertainty in each of the two weighings is $\pm 2.0\%$ or 20 times as great. This comes about because of the functional relationship expressed in equation (2). By making use of Archimedes' Principle, it is possible to capitalize heavily on the high degree of accuracy with which the triple-point liquid density ρ_l is known.

As an example, equation (2) and the typical values mentioned before are used to find the mean for a solid fraction of 0.50. Thus

$$\rho = \rho_l \left(\frac{M_b}{M_l} + 1\right) = 77.017 \left(\frac{117}{2000} + 1\right) = 81.53 \text{ g/l .}$$

The fractional error in ρ is

$$\frac{d\rho}{\rho} = \pm \frac{0.15}{81.53} \text{ or } \pm 0.18\% .$$

From these considerations it may be concluded that the density of hydrogen slush at 0.50 solid fraction can be determined with an uncertainty of less than $\pm 0.2\%$ if a weighing system which is accurate to $\pm 2.0\%$ is used. Figure 3 shows how the uncertainty in slush density will vary for the assumed system as the density itself is varied. A scale of mass fraction solid (sometimes called "quality") is shown for comparison with density. The uncertainty is shown in grams per liter as well as percent of measured mean density.

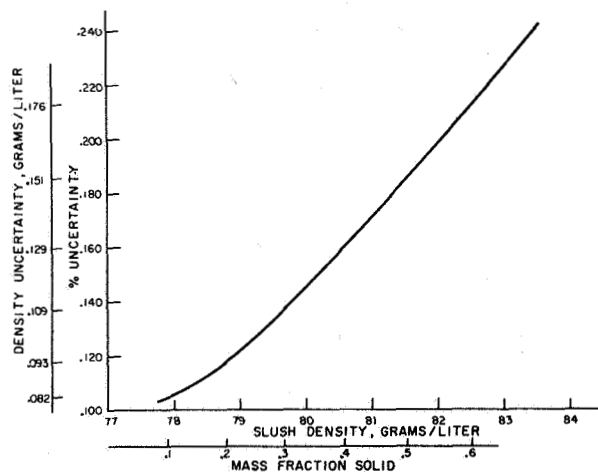


FIGURE 3. GRAPH SHOWING RESULTS OF ERROR ANALYSIS

Figure 4 is a detailed diagram of the slush density cryostat. The container is suspended from a load cell which is located on top of a cylinder above

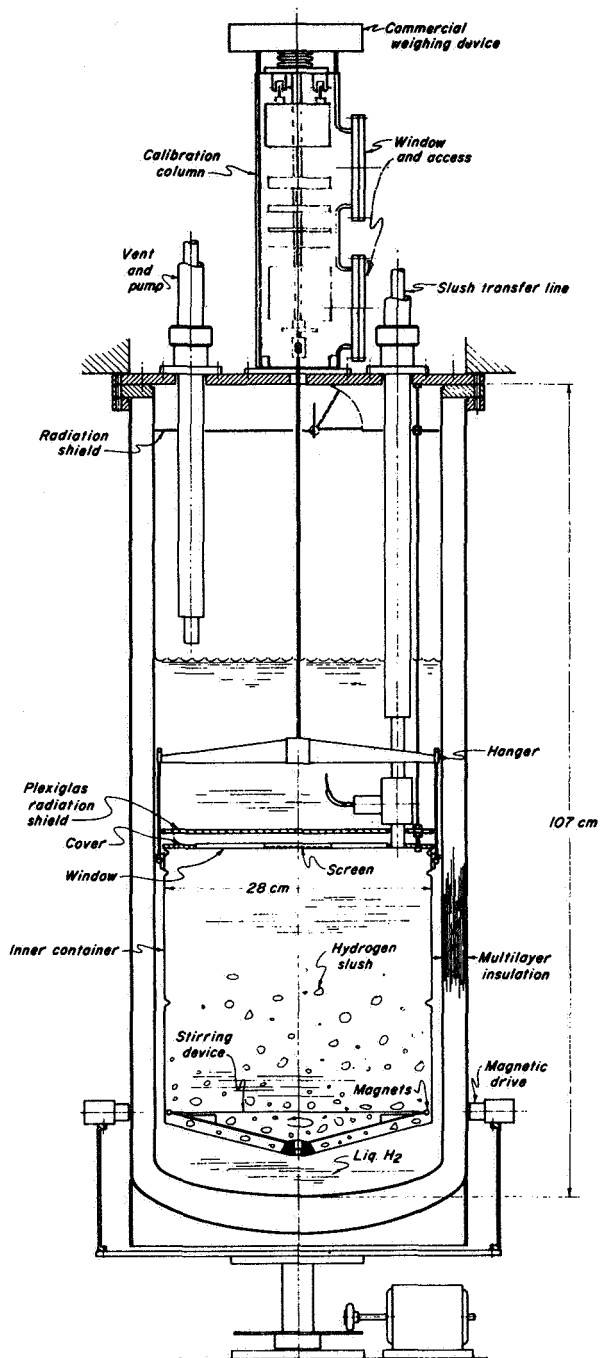


FIGURE 4. DETAILS OF CRYOSTAT FOR DETERMINATION OF HYDROGEN SLUSH DENSITY

the top plate of the cryostat. The cylinder houses a series of calibration masses. Two windows provide observation and access to the dead weight calibration system. The container can easily be lifted from the suspension system by raising it against the cover plate, and one or more of the calibration masses can be substituted. Slush is transferred from the slush generator while the container is in the raised position. The solids are retained while the excess liquid is pumped off. When a convenient solid fraction has been added to the liquid, the final weighing is made.

After a determination of average slush density in the container has been made, it must be correlated with a reading or series of readings from the transfer standard that is being calibrated. There are presently two types of transfer standards available: the Nuclear Radiation Attenuation (NRA) Transfer Standard and the Internal Point Densitometer, both described in this paper. The Internal Point Densitometer is located inside the slush container and is supported from the cover, which serves as a lid when in the raised position. When the container is lowered for weighing, it no longer contacts the cover, so that the cover and attachments to it are not weighed.

The Nuclear Radiation Attenuation Transfer Standard is mounted outside the dewar. This arrangement has many advantages for both calibration and field use.

To maintain a favorable attenuation ratio between hydrogen slush and metal, the cryostat and container walls have been made as thin as possible. Type 316 stainless steel is used for the container and both shells. The outer shell is 0.13 cm thick, the inner shell is 0.08 cm, and the inner container walls are 0.06 cm thick. The attenuation of gamma rays by the total of 0.54 cm of steel will be about the same as the attenuation by the 28 cm of hydrogen slush having an average density of 80 g/l.

Access ports offering less gamma ray attenuation can be provided where the beam passes through the 0.13 cm thick outer walls, but the attenuation ratio without access ports is sufficiently favorable to justify avoiding this complication in the initial fabrication. Easy modification of the outer shell is made possible by providing separate removable vacuum seals for both inner and outer shells at the top plate.

The cryostat is insulated with evacuated multi-layer aluminumized Mylar sheets alternating with porous glass paper. The annular space is 2.5 cm, about 3/4 of which will be filled with the laminae. The resulting 3.8 cm of loosely layered Mylar sheets and

glass paper is not a significant barrier for energetic gamma radiation, but does provide an efficient thermal barrier. Total heat flux through the multilayer insulation will be approximately 2 W out of a total expected heat leak of 15 W. Solid conduction will account for about 6 W, radiation from the top plate about 4 W, and gas conduction about 3 W.

Practically all of this heat will be intercepted by the triple-point liquid surrounding the slush container. This is important since it is impractical to simultaneously weigh and take readings from the transfer standard because the mixture will not be homogeneous unless it is stirred, and accurate weighings cannot be made while stirring.

The small amount of heat which reaches the contents of the container will melt some of the solid hydrogen and continuously change the average slush density. The density thus becomes a function of time, and it will be necessary to determine this time dependence when experimental measurements begin. A preliminary task is to analyze the accuracy with which this can be done. Since there will always be some elapse of time between a density determination and a readout from a transfer standard which is in place and being calibrated, it is apparent that the time dependence of ρ must be known with a high degree of accuracy.

This analysis, which is part of the error analysis for the system, has been carried out and shows that even if generous assumptions are made about the heat leak to the inner container and time elapse between load cell and transfer standard readings, the heat leak correction can be incorporated without addition of any significant new uncertainty.

Most density sensitive transducers (including a beam of gamma rays) will normally sample a relatively small fraction of the slush in the container, and therefore this reading will not indicate the true average density unless the mixture is kept homogeneous during the reading interval. To keep the central part of the container clear of protrusions, a method for stirring magnetically from outside the cryostat was devised. A low-mass rotor inside the container carries slender bar magnets which link flux with heavy permanent magnets carried on a wheel surrounding the cryostat. This magnetic driving wheel can be spun by hand or turned by a small motor operating against a friction disc. Stirring will always be done with the container in its raised and closed position to prevent loss of solids. When the container is lowered for a weighing, the magnetic driving wheel

will be dropped away by means of a simple elevator and lever arrangement so that there will be no magnetic force exerted on the rotor.

Thus the sequence of operations, starting with slush in the container, is as follows:

1. With the container raised, calibrate the weighing system.
2. Lower the container and weigh it.
3. Raise the container and stirring driver.
4. Stir and read the transfer standard.

A check on homogeneity can be obtained by taking several readings of the transfer standard while stirring at slightly different rates for each reading. If the readings are constant, the mixture should be homogeneous. The slush density reference system is now operational, and calibration of transfer standards will be started in the near future.

NUCLEAR RADIATION ATTENUATION TRANSFER STANDARD

A 450 liter slush generator has been in use for the past year. A commercial densitometer based on gamma ray attenuation has recently been installed on the slush generator. Initial results obtained with this device have been very encouraging.

The densitometer consists of a 4 Ci, 0.663 MeV, cesium 137 source; an ion chamber detector; an impedance matching unit; and an instrument console. The signal from the densitometer is measured with a digital volt meter and recorded on a strip recorder. Figure 5 shows the position of the source and the detector with respect to the slush generator. The beam must penetrate 1.12 cm of stainless steel, 1.27 cm of aluminum, and 76 cm of liquid or slush hydrogen. About one-half of the attenuation of the beam takes place in the hydrogen.

Figure 6 shows the experimental results obtained with the densitometer. The millivolt output of the densitometer is in each case the mean value of at least 10 digital voltmeter readings. The density was determined by three different methods, depending on the state of the hydrogen.

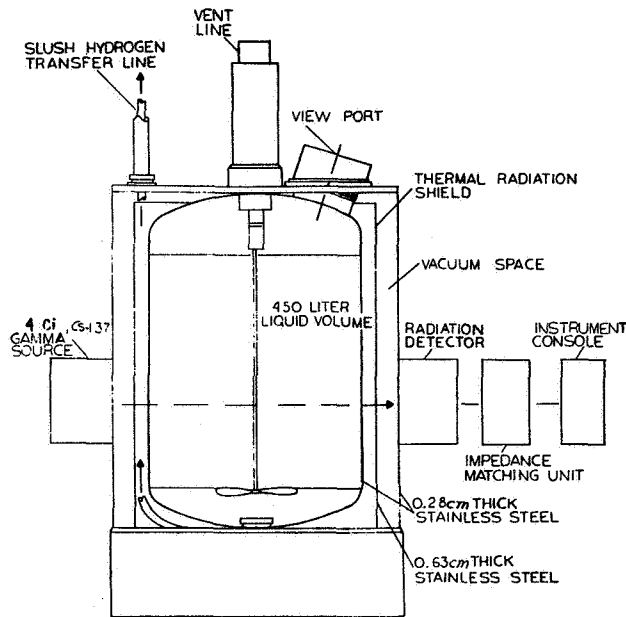


FIGURE 5. 450-LITER HYDROGEN SLUSH GENERATOR WITH NRA DENSITOMETER

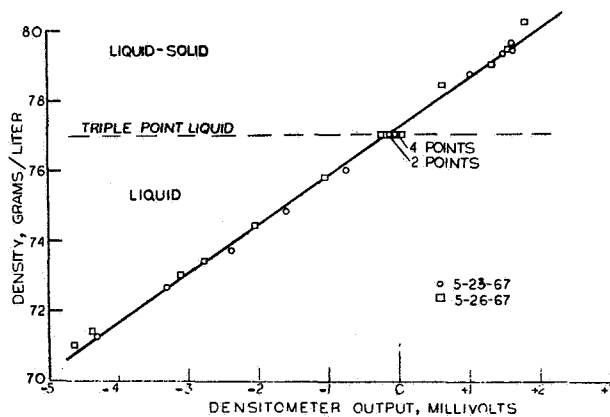


FIGURE 6. NRA DENSITOMETER RESULTS

In the liquid region at pressures above the triple point, the density was determined by measurement of the vapor pressure over the liquid. The triple-point liquid condition was determined by making a small amount of solid in the slush generator, mixing the solid particles thoroughly by stirring, and then taking the densitometer reading as the last of the solid particles settled past the region penetrated by the beam.

The density in the liquid-solid region was determined calorimetrically. After a densitometer reading was taken on stirred slush formed by the freeze-thaw production process [3], a heater in the bottom of the generator was energized until the triple-point liquid condition was achieved. The solid fraction, and hence the density, was then determined from the sum of the heater energy and heat leak.

The densities used in the liquid region are those reported by Roder [1], and the triple-point solid density is given by Dwyer, et al., [4].

The standard deviation of the measured densities about the least squares straight line in Figure 6 is 0.17 g/l. The slope of the curve does not change in passing from the liquid to the liquid-solid region, so it is possible to predict densities in the liquid-solid region by linear extrapolation of a liquid region calibration.

The uncertainty of the measured density values is estimated as a few parts in 1000. Since this uncertainty is of the same order as the scatter in the results, further evaluation of the NRA densitometer awaits completion of the density reference system.

INTERNAL POINT DENSITOMETER

A hydrogen slush densitometer based on previous research contracts, developed first for liquid oxygen and later modified for liquid hydrogen, has been further modified for slush hydrogen. The ORTEC slush hydrogen densitometer consists of three encapsulated surface barrier radiation detectors and sealed strontium-90 sources, and three channels of modular electronics instrumentation for processing detector signals.

Each detector probe assembly is composed of a 50 mm² active area 500- μ thick totally depleted surface barrier detector housed in a stainless steel capsule having a 0.051 mm (0.002 in.) thick stainless steel window. The source housing, also fabricated of stainless steel, contains a sealed 15 mCi strontium-90 beta source. For additional safety, a 0.025 mm (0.001 in.) thick stainless steel window has been fabricated into the source housing. The detector probe-source housing assembly is designed so that axial and lateral geometry alignment is constant, thus requiring only source-to-detector distance adjustments.

Beta particles from the source are absorbed by the detector, thereby producing minute electrical pulses or charges. These pulses, in the form of electrical current, are fed through the preamplifier to the linear amplifier. The linear amplifier shapes and further amplifies the pulse, which is then fed to the discriminator where it is determined to be either above or below a given energy threshold. The discriminated pulses are converted to a dc signal corresponding to the pulse rate, and finally re-converted to a dc output that is to be calibrated to indicate the percent solid fraction in the liquid hydrogen slush. A block diagram of a channel is shown installed in the reference system in Figure 7.

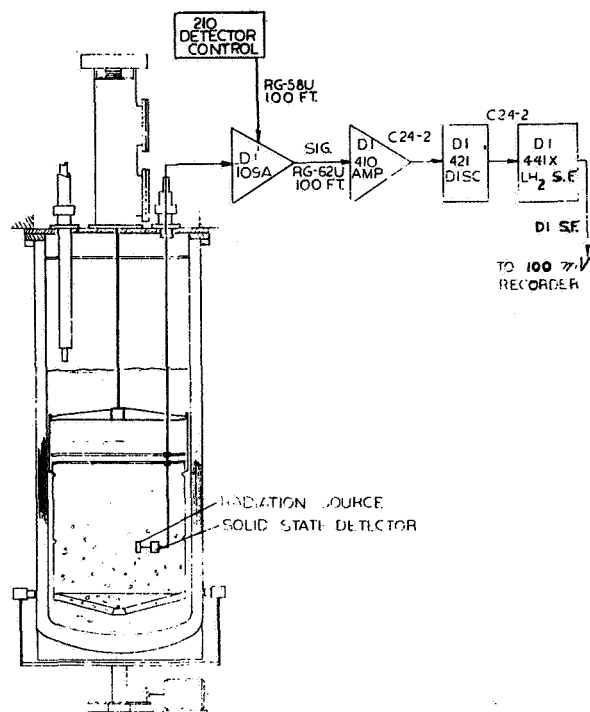
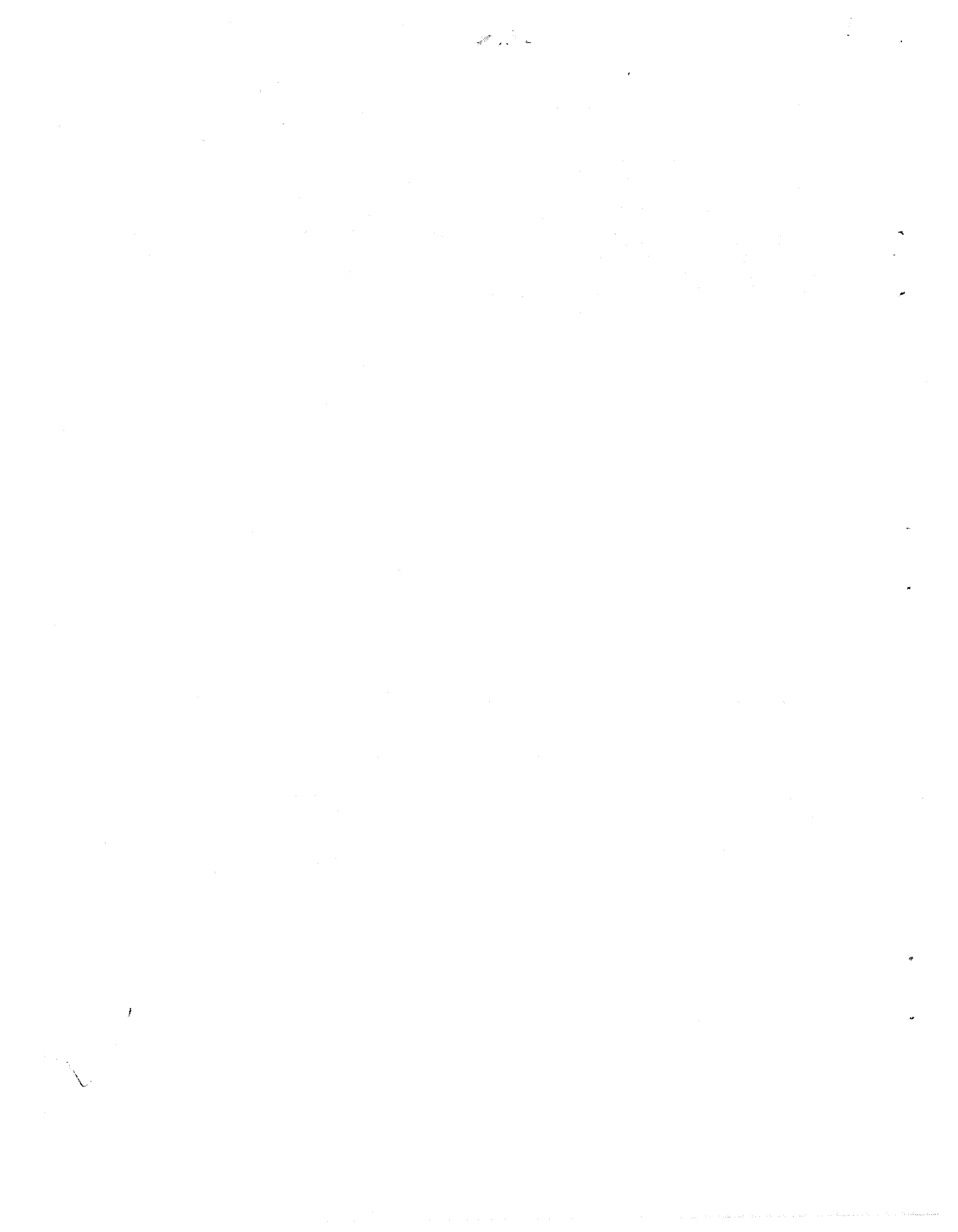


FIGURE 7. ORTEC SLUSH HYDROGEN DENSITOMETER

REFERENCES

1. Roder, H. M.; Weber, L. A.; and Goodwin, R. D.: Thermodynamic and Related Properties of Parahydrogen, from the Triple Point to 100° K at Pressures to 340 Atmospheres. NBS Monography 94, 1965.
2. Wilson, E. B., Jr.: An Introduction to Scientific Research. McGraw-Hill Book Co., Inc., 1952.
3. Mann, B. D.; Ludtak, P. R.; Sinat, C. F.; and Chelton, D. B.: Liquid-Solid Mixtures of Hydrogen Near the Triple Point. Advances in Cryogenic Engineering, Plenum Press, New York, N. Y., vol. 11, 1966, pp. 207-217.
4. Dwyer, R. F.; Cook, G. A.; Berwaldt, O. E.; and Nevins, H. E.: Molar Volume of Solid Parahydrogen Along the Melting Line. J. Chem. Phys., vol. 43, 1965, p. 801.



PRESSURE TRANSDUCERS FOR ENVIRONMENTAL EXTREMES

By

Harlan S. Harman

SUMMARY

This review covers two research programs. One of them discusses design development and fabrication of an experimental high temperature, high frequency response pressure transducer for combustion instability studies requiring frequency response of 20 kHz in an environment where temperature reaches 4144° K (7000° F) and the heat flux can be as high as 8200 W/cm² (50 Btu/in.²-sec). The second program covers the design, development and fabrication of a cryogenic pressure transducer for static and dynamic measurements at liquid helium temperatures of 4° K.

HIGH TEMPERATURE, HIGH FREQUENCY RESPONSE PRESSURE TRANSDUCER

The accurate measurement of the amplitude and frequency of dynamic pressures in a rocket combustion chamber during unstable combustion has been a problem for several years. The required temperature and frequency response capabilities of a pressure transducer operating in an unstable combustion environment were such that they could not be met with existing transducers. Commercially acceptable transducers would be destroyed by the high heat flux of up to 8200 W/cm² (50 Btu/in.²-sec) generated in the chamber during unstable combustion.

Past techniques used to cool the pressure sensing portion of pressure transducers have been unsatisfactory. These techniques were as follows:

1. Water-cooled flush-mounted diaphragm. This approach used a nucleate boiling technique of storing water on a flush-mounted diaphragm to act as a flame shield for a strain gage type sensing element. The proper frequency response was achieved, but the transducer diaphragm burned through during unstable combustion.

2. Small gas passage technique. In this technique the pressure sensing element is mounted a short

distance away from the high temperature region in a small opening in the combustion chamber. Satisfactory cooling of the sensing element is achieved with this technique; however, a considerable reduction in frequency response does result.

3. Spray cooling technique. Cooling is accomplished by flowing water or other fluid past a sensing element and injecting the flow into the combustion chamber. To adequately protect the sensing element from the high heat flux environment required an excessive amount of fluid to be injected into the combustion chamber.

To achieve high frequency response, the transducer must be flush mounted in the combustion chamber. Past experience with the above cooling methods showed that a new cooling technique would have to be developed to satisfactorily meet this requirement.

A concept of using mass transfer or transpirational cooling of a dense porous plug appeared to be the most promising technique of adequately protecting a flush mounted pressure transducer from the high temperature environment. Transpirational cooling is accomplished by flowing a gas through a porous material. A theoretical analysis of this cooling technique shows that the temperature difference between the plug material and the coolant gas is very small, and the heat conducted through the plug material is carried away by the coolant.

The research effort centered around the development of the transpirational cooling technique that is necessary for having a reliable high temperature, high frequency response pressure transducer capable of continuous operation in unstable combustion environments. Figure 1 is a sectional view of the pressure transducer developed from this research effort. This view shows the important components in the transducer. The porous plug at the upper end of the transducer is flush-mounted in the rocket chamber at the point desired. Pressure (both static and dynamic) in the rocket chamber acts upon the porous plug, and the force is transmitted down the inner column to the strain gage sensing bridge at the lower

end of the transducer. Semiconductor gages were used rather than resistance gages to achieve the high output required with the low strains.

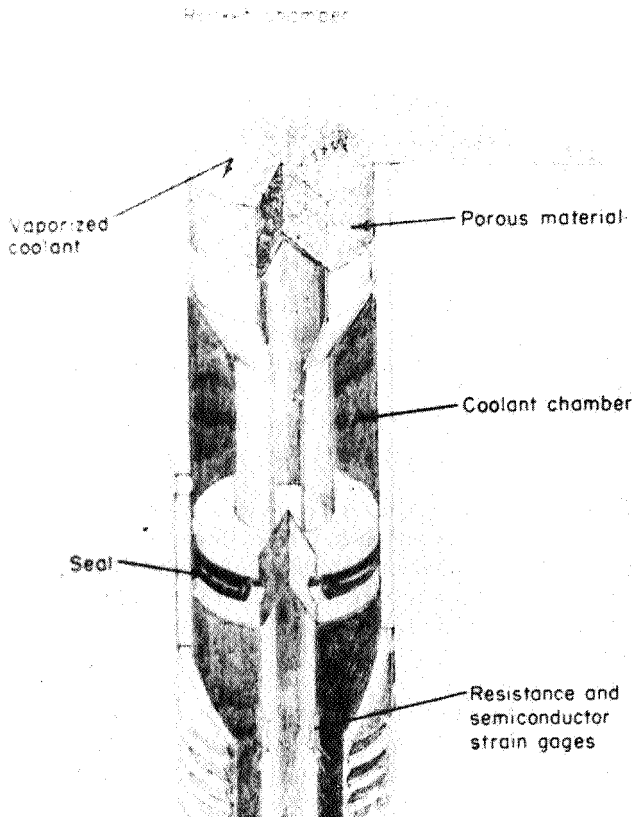


FIGURE 1. CONCEPTUAL DESIGN

The steady or transient heat fluxes are kept from the sensing element by bleeding a coolant, compatible with the combustion process, through the porous material. Because of the very small passages in the porous material, essentially the transient pressures will "see" the plug as a solid material. Thus, imposed strains in the lower portion of the column are the same as if the plug were solid. The coolant, either gaseous helium or hydrogen, is introduced through the center of the inner column at a point below the porous material and at a steady pressure higher than that encountered in the combustion instability regions. Figure 2 shows a sectional view of the transducer. A No. 29 hypodermic needle 0.0178 cm i.d. (0.007 in. i.d.) is used to meter the flow and to act as a critical flow passage to maintain the flow at a constant mass flow rate. Although in this design some changes in output occur with changes in coolant pressure, this error is small and may be eliminated

by taking a zero reading after full coolant pressure is established. The coolant supply pressure must be sufficiently high that critical flow through the orifice is maintained at the highest rocket chamber pressures.

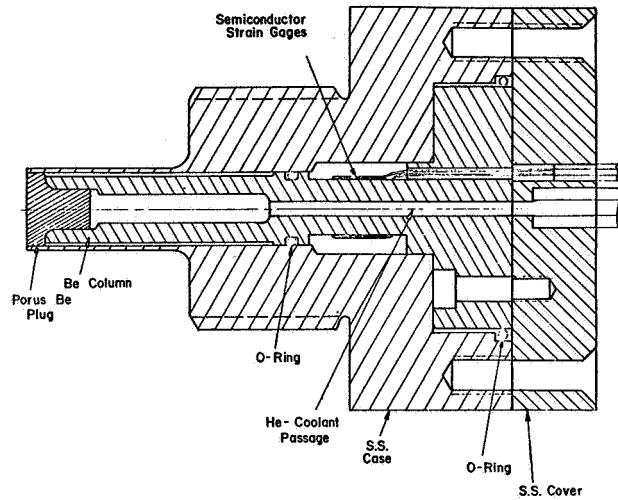


FIGURE 2. SECTIONAL VIEW OF TRANSPIRATIONALLY COOLED PRESSURE TRANSDUCER

Using a small column in compression and maintaining low strains for the maximum design pressure allows for attaining a very high natural frequency for this system. In addition, beryllium, which has an exceptionally high stiffness-to-weight ratio, was selected so that both the porous plug and inner column would have a high natural frequency.

TYPICAL SPECIFICATIONS

Minor variations in material properties, tolerances, strain gage characteristics, etc., require that calibration and response characteristics of each transducer must be determined experimentally. However, in general, typical specifications for this transpirationally-cooled pressure transducer are as follows:

Range	0 - 1379 N/cm ² (0 to 2000 psig)
Output-sensitivity at least	0.0046 mV/V-psi
External Vibration Sensitivity	
Axial	less than 0.012% full scale per peak g
Transverse	less than 0.007% full scale per peak g

Thermal Shift from
299.8° to 327.5°K less than 0.14% full scale
(80° to 130° F)

Although the thermal shift was determined for the ranges 299.8 to 327.5°K (80° to 130°F), the temperature at the sensing bridges is not expected to vary more than 11.0°K (20°F).

Combined error caused by thermal shift non-linearity, hysteresis, and repeatability, is $\pm 3\%$ full scale. Most of this error is hysteresis and is attributed to the O-ring seals. With a modified O-ring groove that has been incorporated into the design, this error is expected to vary by less than $\pm 2\%$ full scale.

Resonant Frequency (axial)	74 kHz
Frequency Response	Flat or 1% to 7.5 kHz

These specifications reflect the values determined for the two prototype transducers fabricated at the end of this program and supplied to NASA.

The development of this concept into a useable transducer involved three parallel efforts, each in a different technical field. These efforts are (1) thermal studies, (2) porous material development, and (3) mechanical design and evaluation of transducers. These subjects will be discussed only briefly, but full details are available to those having further interest.

The work in the thermal phase was directed toward evaluating the cooling concept and determining the relation between the particle size and porosity of the porous plug and the coolant flow rate required to provide adequate cooling for the transducer. The plugs are fabricated by compaction of nearly spherical beryllium or tungsten particles into a body. The principal variables affecting the flow are average particle size, particle size distribution, and degree of compaction. This last variable is correlated in practice with percent of theoretical density of the metal being used. An effort was made early in the program to develop a correlation from flow tests with regards to the effect on flow of the particle sizes and densities of the porous material. Thus, tungsten plugs of only two particle sizes and of various densities were fabricated and flow tested.

For the transducer development, two kinds of plugs were selected from those available for thermal

evaluation on the basis of gas permeability. This choice proved to be correct from evidence revealed during the thermal tests. The two kinds of porous plugs were the 115 μ , 83.5% dense tungsten plug and the 50 μ , 77.4% dense beryllium plug.

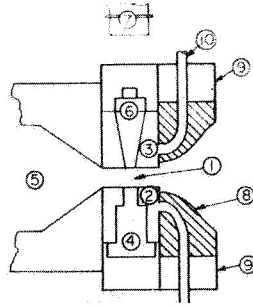
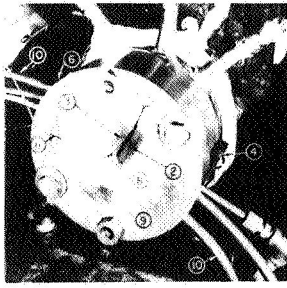
SIGNAL TRANSMISSION

The transducer senses the rocket chamber pressure through the elastic response of the beryllium parts. The gaseous coolant is used for the sole purpose of thermal protection. Any signal transmission in the gas passage within the plug only tends to complicate the phenomenon and might distort the signal being measured. In the state of the art, it is not clear whether there is any interaction between the signals transmitted through the solid and the signal transmitted through the gas within the passages in the solid, and what is the effect on the transducer accuracy, if any. Under this circumstance it was believed reasonable to attempt to minimize the signal transmitted through the gaseous medium. An attempt was made to analyze the signal transmitted in a gas passing through a porous material. The details of this analysis and its application to the transducer are available in the final report of the contractor [1]. The same applies to many other details in the following sections of this paper [1, 2]. The analysis showed that the signal transmitted through the gas within the porous plug is not significant in practical plug materials as are being used in the transducer.

Thermal tests of both plugs and complete transducers were carried out to determine the amount of coolant required for safe operation; to estimate the temperature distribution in the porous materials; to study the coolant system so that an adequate amount of gas is supplied; and also to determine peak temperature at the sensors. One third or more of the total development effort in this contract was used in the development of a suitable porous plug. Tungsten and beryllium plugs were successfully manufactured.

ROCKET MOTOR TEST ARRANGEMENT

A brief description of rocket motor test arrangement is shown in Figure 3. The rocket motor used in the transducer testing part of this program consists of a 3.81 \times 15.2 cm ($1\frac{1}{2}$ \times 6 in.) cylindrical combustion chamber, an injector with six oxidizer jets impinging onto a central fuel jet, a convergency nozzle which provides a rectangular throat, and a transducer test section mounted downstream of the nozzle. Gaseous hydrogen and oxygen propellants were used in a 5 to 1 weight ratio.



1. Rectangular nozzle throat extension
2. Water-cooled transducer nozzle block
3. Water-cooled window block, also a calorimeter
4. Pressure transducer
5. Combustion chamber
6. Quartz window
7. Radiation pyrometer, "Rayotube"
8. Refractory ceramic potting material
9. Brass retaining body
10. Cooling water lines to nozzle blocks
11. Ignition wire for rocket combustion

FIGURE 3. ROCKET MOTOR TEST ARRANGEMENT

INNER COLUMN OF TRANSDUCER

The inner column element (Fig. 4) is the most important component in the transducer. The response

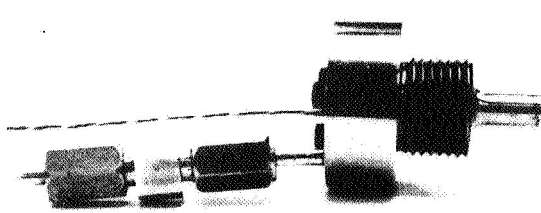
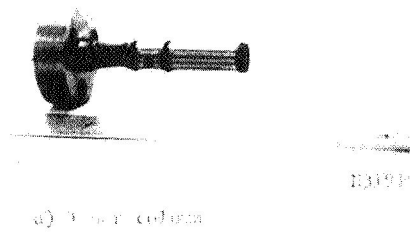


FIGURE 4. INNER COLUMN AND ASSEMBLED TRANSDUCER

of this element to the pressure in the rocket chamber is measured and interpreted as pressure. The strains created in this column by the pressure must be high enough to produce the required output while at the same time be low enough to maintain the high axial response frequency of the element. The geometry of this element is such that it responds only to axial loads. Lateral motions are minimized because the column is guided by the porous plug and seals. In addition, bending strains can be completely cancelled out in the sensing bridge by proper location of the strain gages.

FREQUENCY RESPONSE

Pressure pulses impinging on the surface of the porous plug cause compressive strains in the inner column. These strains are imparted to the strain gages, and resulting changes in resistance are monitored and interpreted as pressure amplitude. Errors in the output signal occur as the frequency of the pressure signal approaches the resonant frequency of the column. In these units the damping is very small (damping ratio less than 0.05), and the output amplitude is larger by 1% when the frequency of the pressure signal reaches 1/10 of the column resonant frequency. When output errors of less than 1% are desired, and the maximum frequency of the pressure signal is 20 kHz, it is necessary to have a column resonant frequency in excess of 200 kHz.

In general, three choices are available for increasing the resonant frequency of a column element. These choices are:

1. Use a material with a higher stiffness-to-weight ratio.
2. Shorten the length of the column.
3. Increase the stiffness by increasing the lower column area.

Beryllium was selected initially for the inner column because of its high stiffness-to-weight ratio, and later it was also selected as the best choice based on the stiffness-to-weight ratio of the applicable materials.

Shorter length columns were investigated but it was found that if the column is shortened appreciably, fabrication and assembly problems are more severe and larger temperature excursions at the strain gage bridge are possible. Therefore, it was decided not to reduce the length of the inner column.

The only route left open to increase the resonant frequency of these units was to increase the column cross-sectional area at the base. A column area of 0.175 cm^2 (0.0272 in.^2) was selected (increase of 75%) to insure a minimum output of 30 mV at maximum rated pressure. With a 75% increase in the column stiffness the resonant frequency should increase 32% to approximately 100 kHz.

INSTALLATION AND COMPENSATION OF THE STRAIN GAGE BRIDGE

Because of small size and output sensitivity desired for the transducer, semiconductor strain gages of small gage length and moderate resistance were selected as the most desirable sensing element. The resistance of all gages was measured before installation to allow selection of sets of four gages nearly equal in resistance. The selection of matched sets was considered important to avoid the need of excessive compensation.

The gages were installed in a Poisson bridge arrangement to measure axial strain and provide temperature compensation. The first fully instrumented prototype transducer with a 77.4% dense porous beryllium plug and a $127\text{-}\mu$ (5-mil) coolant flow orifice was thermally tested in the rocket motor at the conditions as follows: chamber pressure: 276 N/cm^2 (400 psig); heat flux 4140 W/cm^2 ($25.3 \text{ Btu/in.}^2\text{-sec}$); duration of test: 30 sec; plug surface temperature: 888.7° to 949.8° K (1140° to 1250° F); coolant supply pressure: 1411 N/cm^2 (2050 psig). In addition, a thermocouple was inserted in the vent hole in the lower chamber until it contacted the lower flange of the O-ring seal. The temperature of this point, monitored during each test, did not change. That is, it remained at room temperature, thus indicating that there was sufficient coolant flow for these conditions. Inspection of the transducer after the tests revealed only minor erosion of the surface of the porous plug.

CRYOGENIC PRESSURE TRANSDUCER

The testing of rocket engines that use cryogenics requires accurate measurements of static and dynamic pressures at temperatures down to that of the liquid helium (4° K). The transducer should be small, lightweight and capable of being inserted in a standard boss; it should be capable of reaching thermal equilibrium quickly, be insensitive to dynamic temperature changes, and should be capable of responding to high

frequency pressure oscillations. Accurate measurement of pressure parameters is important because it permits design verification of hardware, auxiliary equipment, pumps, flow, plumbing systems, etc., and it permits design modification of the engine, fuel, oxidizer, thrust chamber conditions and control systems. It permits detection and analysis of malfunctions of subsystems.

Two approaches were considered to meet these criteria during this program. One approach was the use of gallium antimonide as a hydrostatic pressure sensitive material, and the other approach was the use of silicon gages bonded to metallic pressure sensitive diaphragms.

Initially it was proposed to fabricate elements of the gallium antimonide from bulk crystal material. This proved impractical for two reasons. First, in order to obtain a bridge resistance of 100Ω or greater, a length-to-area ratio of 20,000 to 1 was required. Second, assuming these high resistivity crystals could be grown, elements fabricated from them would have extremely nonlinear "resistance-to-temperature characteristics," and temperature compensation over a wide range, therefore, would not be practical. As an alternative, high resistance elements were produced by diffusion techniques. Surface diffusion results in a very thin (approximately 1μ) surface layer of selected gallium antimonide material electrically isolated from a thicker, mechanically strong substrate through P - N junction action. This shallow depth permits fabrication of sensor elements having practical length, width, and resistance values, while at the same time allowing for the use of impurity levels that are high enough to insure linear resistance to temperature relationships. A satisfactory process for making N and P type gallium antimonide surface layers was developed. The resistance of the N-type gallium antimonide increases by roughly 1% per 689 N/cm^2 (1000 psi) hydrostatic pressure.

The P-type exhibited no appreciable hydrostatic pressure sensitivity. A working transducer using the P and N type GaSb was never successful because of the difference in the temperature resistance characteristics of the P and N type elements. This problem is not insurmountable, but requires more time for the development of technique in fabrication. During the course of the development it was noted that balco nickel wire had a resistance - temperature characteristic corresponding to that of N-type GaSb (Fig. 5). This material was substituted for the P-type GaSb for completing the bridge. Three transducers were then fabricated (Fig. 6). They were just recently received and therefore have not been evaluated.

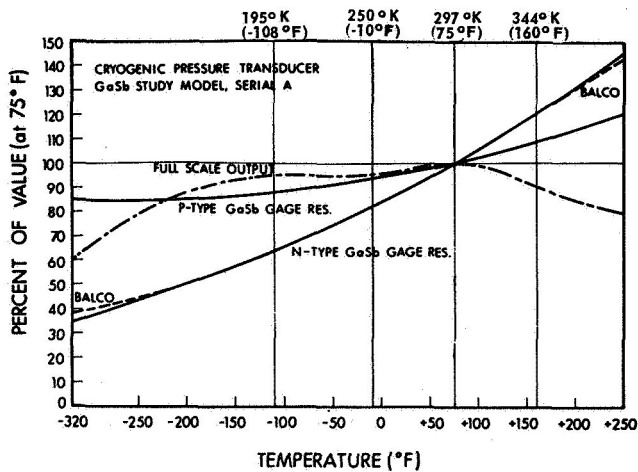


FIGURE 5. BALCO WIRE COMPARED WITH N-TYPE GaSb GAGE RESISTANCE

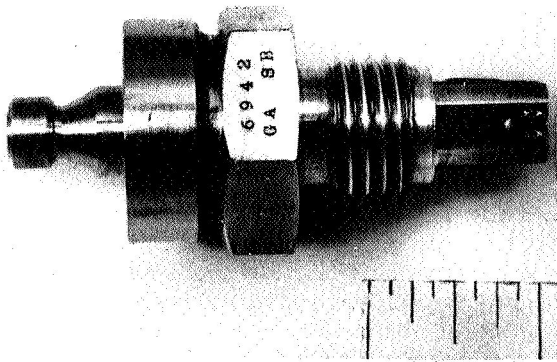


FIGURE 6. GaSb TRANSDUCER

The second approach, the use of silicon strain gages, required careful consideration of not only the mechanical and electrical properties of the silicon elements, but also the mechanical properties and geometry of the sensing diaphragm. A number of approaches using single chip silicon gages bonded to diaphragms were unsuccessful as a result of large changes in compression stresses sensed by the compression gages at low temperature. These changes were caused by diaphragm structural and dimensional changes with temperature and from the increased strength of bonding agents between gage and diaphragm at low temperatures.

The next approach was to use heavily doped diffused silicon strain gages bonded to nispan c diaphragms in a four active arm bridge configurations.

Diffused silicon gages with surface impurity concentrations of $1.4, 3,$ and 5×10^{20} boron atoms/cm³ were produced (Fig. 7). These gages bonded to the nispan c diaphragm and excited with a constant current power supply were capable of stable operations over a range of 3.70° to 394° K (-453° to $+250^\circ$ F) (Fig. 8). Sensitivity shifts of 2 to 3% per 55.6° K (100° F) from 3.70° to 394° K (-453° to $+250^\circ$ F) were proven feasible with a minimum of compensation circuitry. Sensitivity of less than 1% per 55.6° K (100° F) was achieved over narrow temperature spans. A zero shift of 1 to 2% per 55.6° K (100° F) was attained from 3.70° to 394° K (-453° to $+250^\circ$ F). Figure 9 shows typical transducer elements. Figure 10 shows a disassembled transducer. Three prototype transducers were furnished for further evaluation (Fig. 11). Figure 12 shows a typical performance curve when transducers are subjected to liquid nitrogen.

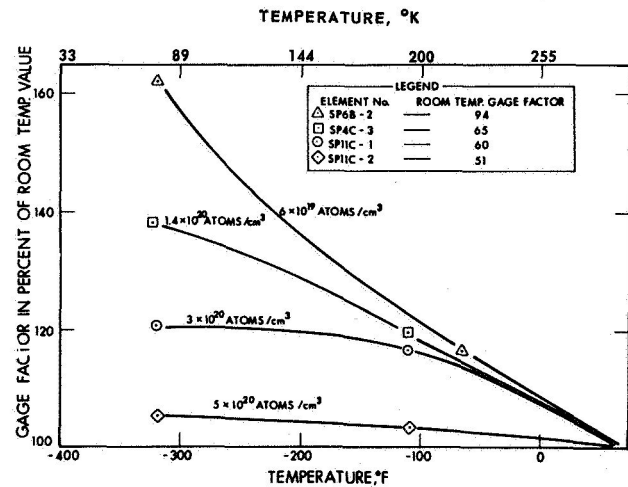


FIGURE 7. GAGE FACTOR CHANGE vs TEMPERATURE

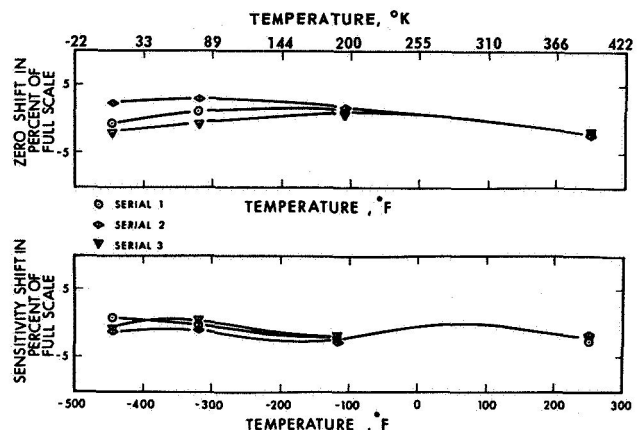


FIGURE 8. CRYOGENIC PRESSURE TRANSDUCER — ZERO AND SENSITIVITY SHIFT WITH TEMPERATURE

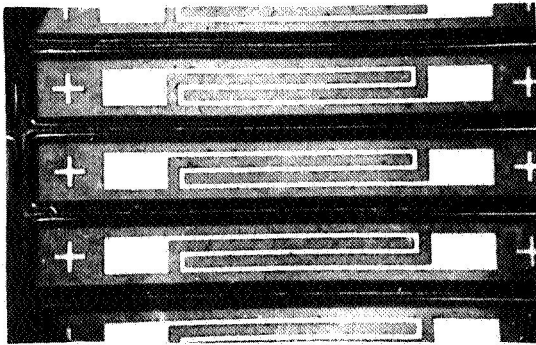


FIGURE 9. TYPICAL TRANSDUCER ELEMENTS

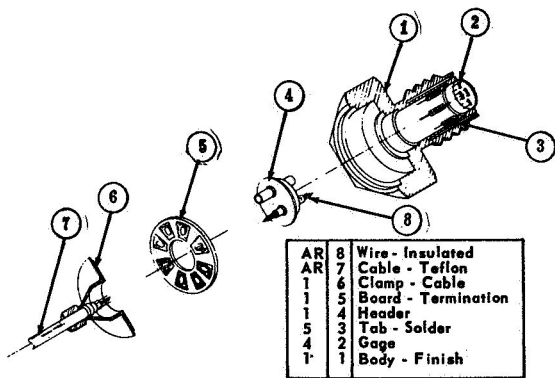


FIGURE 10. DISASSEMBLED CRYOGENIC PRESSURE TRANSDUCER

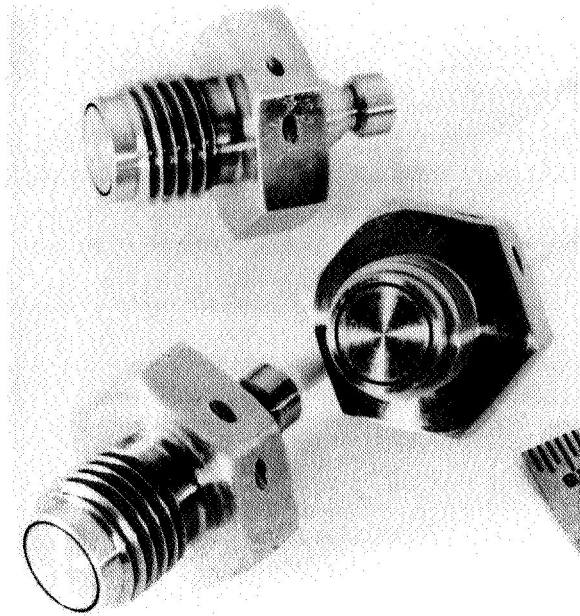


FIGURE 11. COMPLETED TRANSDUCERS

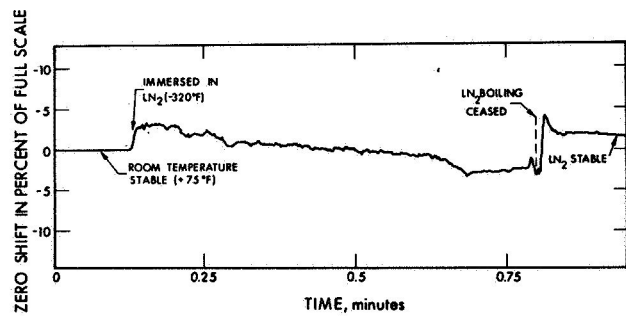


FIGURE 12. TYPICAL PERFORMANCE CURVE (RESPONSE OF TRANSDUCER ZERO OUTPUT TO STEP CHANGE IN TEMPERATURE)

REFERENCES

1. Design, Development and Fabrication of an Experimental High Temperature High Frequency Response Pressure Transducer. Final Report, NASA (MSFC) Contract No. NAS8-11933, Battelle Memorial Institute, Columbus, Ohio.
2. Study and Investigation Design, Development and Fabrication of A Cryogenic Pressure Transducer. Final Report, NASA (MSFC) Contract No. NAS8-11934, Electrical-Optical Systems, Inc., Pasadena, California.



PRECEDING PAGE BLANK NOT FILMED.

THE USE OF THE MOSSBAUER EFFECT AND LASER INTERFEROMETRY TO DETERMINE EXTREMELY SMALL AMPLITUDES FOR VIBRATION MEASUREMENTS AND CALIBRATIONS

By
Helmut G. Lackner

N 68-30628

SUMMARY

Two methods for making an improvement of the state of the art in obtaining precise vibration measurements and calibrations are presented in this paper. The discussion concentrates on vibration tests on scale models, and each test often requires making measurements and calibrations of amplitudes that are much smaller than an optical wavelength. The two independent methods described in this paper allow for collecting data well beyond the results obtained by conventional techniques of measuring extremely small amplitudes. One method makes use of the Mössbauer Effect (recoil-free emission and absorption of gamma rays): the extremely sharp resonance lines are dissolved by Doppler shift and can be used for measuring velocities of a fraction of a millimeter per second. This method is used to obtain vibration measurements by measuring and comparing velocities. Since the peak of a Mössbauer line or the peaks of its hyperfine structure are fundamental constants expressed in velocity, a simple calibration technique for electro-mechanical oscillators has been developed where the instantaneous velocity of the oscillating object is compared with a Mössbauer line. With this method, vibration measurements and calibrations can be performed both in the optical and the suboptical range. The other method makes use of refined laser interferometry where monochromaticity, coherence and intensity of laser light are used to produce a stable photocurrent in which the ratio of its frequency components depends on the vibration amplitude. Both methods will allow reaching minimum amplitudes of a few angstrom units with an estimated uncertainty of 2%.

INTRODUCTION

Vibration measurements and calibrations frequently need to be performed in an amplitude range that is too small to be covered by conventional methods, especially if one has to investigate the behavior of scale models that are excited with alternating forces

of much higher frequency than those to which the original object would be exposed. The amplitudes of the responding oscillations have to be decreased accordingly to maintain a realistic simulation, for example, to obtain information about the g-load to be expected. Obtaining data is sometimes difficult because commercial instruments to measure vibration amplitudes below one tenth of a wavelength of light do not exist, or are experimental setups for the laboratory only. However, vibration measurements in the amplitude range below one tenth of an optical wavelength are of great importance for vibrational investigations of scale models.

Our research, therefore, concentrated on methods with which vibration amplitudes from the optical range down to the order of angstrom units could be measured, and methods with which calibrations could be performed. Two completely independent methods which supplement each other were considered: one applies the Mössbauer effect, the other makes use of refined laser interferometry.

MÖSSBAUER EFFECT

The Mössbauer effect is the phenomenon of recoilless resonance fluorescence of gamma rays from nuclei bound in solids. It is characterized by the fact that under certain temperature limitations a nucleus that is embedded in a lattice and is emitting or absorbing a gamma quantum does not recoil because the crystal as a total represents the recoiling mass.

Since the mass of the crystal is infinitely larger than the mass of the nucleus, the recoil energy for the nucleus vanishes. Under this condition the emitted or absorbed gamma line keeps its natural frequency because it is not shifted by the recoil of the nucleus, and furthermore, this gamma line maintains its natural linewidth because it is not broadened by the thermal Doppler effect (Fig. 1). (The thermal Doppler effect is necessarily connected with a transfer of an impulse to an individual nucleus, and this cannot happen for a Mössbauer Line.) However, the

movement of the whole crystal causes a Doppler shift (Fig. 2). Because of the extremely sharp resonance lines, a relative movement of emitter and absorber of only a fraction of a millimeter per second will introduce a Doppler shift from which a perfect resolution of the natural line profile can be obtained.

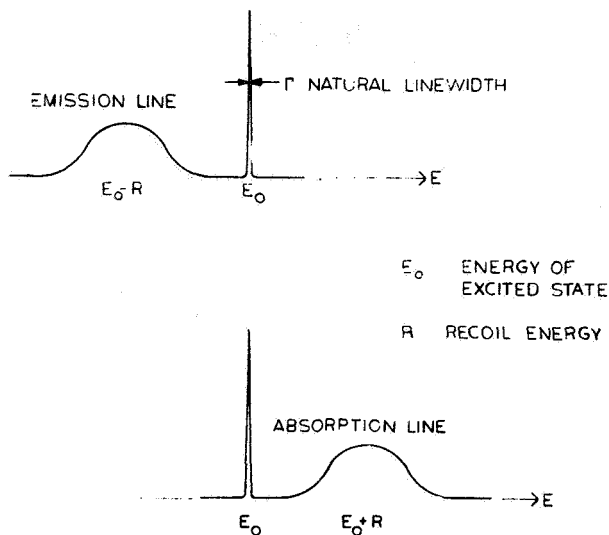


FIGURE 1. MÖSSBAUER LINE AND EMISSION AND ABSORPTION LINE

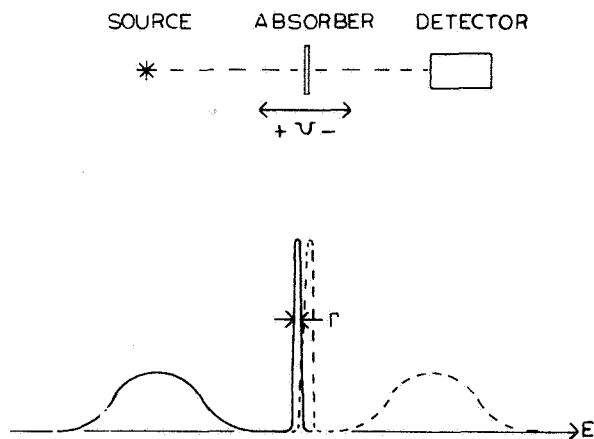


FIGURE 2. PRINCIPLE OF MÖSSBAUER APPARATUS AND DOPPLER-SHIFTED GAMMA LINE

This method does not provide a direct measure of the absolute energy of a line, but it is extremely sensitive in detecting line shifts. In the case of Fe^{57} , for example, the energy of the gamma ray is known to be 14.36 keV with an uncertainty of ± 10 eV, but differences in the energy as small as 10^{-10} eV can be readily measured. Relative changes in energy can be measured with the extreme accuracy of $\frac{\Delta E}{E} = 10^{-13}$.

That means that the energy of the gamma ray is defined to within 1 part in 10^{13} , and thus it is the most accurately defined electromagnetic radiation available for physical experiments.

This extremely sensitive energy resolution makes the method ideally suited to measure the interactions of the surrounding electrons and the external fields with the nuclei, whereby three important phenomena associated with the nuclear hyperfine structure have to be considered: the isomer shift, the quadrupole splitting, and the nuclear Zeeman effect.

Emission and absorption lines are only centered at the same energy if the corresponding nuclei are in similar environments. If this is not the case, for example, by a change in the electrostatic interaction between the nucleus and its electron shell that might arise from a change in valence, a shift of the nuclear levels will result and manifest itself in a zero velocity shift of the resonance curve, which is called isomer shift. If both source and absorber are at rest, little or no resonance will be observed. To re-establish resonance, the absorber or the source is moved with a certain velocity. In this special case of Co^{57} diffused into palladium as source, and stainless steel as absorber, it is -0.26 mm/sec (Fig. 3). (By definition a positive sign stands for approaching, a negative sign for departing source and absorber). The velocity between source and absorber is a measure of energy shift. Therefore, it is usual to express the small energies in Mössbauer experiments in terms of velocity.

Quadrupole splitting is a split in the nuclear levels as a result of the interaction of the nuclear quadrupole moment with the gradient of the electric field arising from other charges in the crystal (Fig. 4). It reflects the deviation of the nucleus from spherical symmetry. Quadrupole splitting is exhibited by different compounds of Mössbauer isotopes. In this example the source is again Co^{57} ; the absorber is crystalline ferrous sulfate.

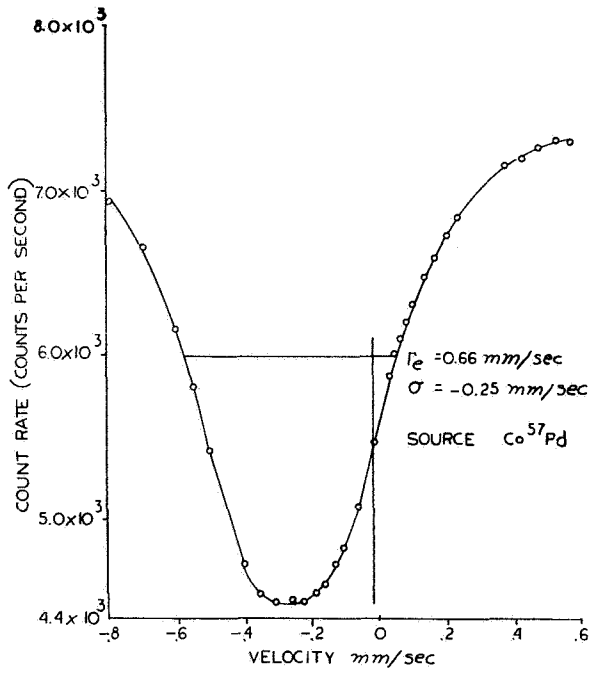


FIGURE 3. CALIBRATION SPECTRUM FOR STAINLESS STEEL ALLOY 310 ENRICHED

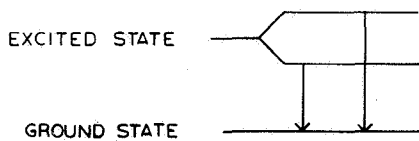
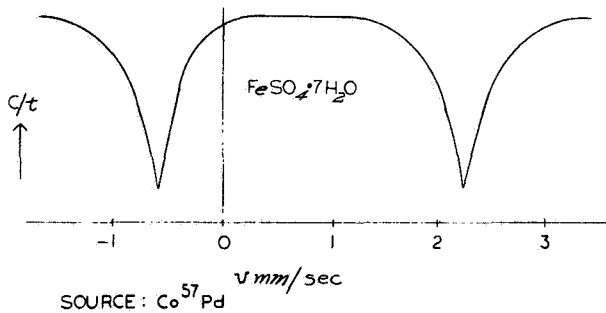


FIGURE 4. QUADRUPOLE SPLITTING

In the case of the Nuclear Zeeman Effect, gamma ray transitions are observed between two nuclear levels that both exhibit magnetic hyperfine

splitting (Fig. 5). The gamma lines correspond to transitions from a particular magnetic sublevel of an excited nuclear state to a sublevel of a ground state. This magnetic hyperfine splitting is caused by the interaction of the nuclear magnetic dipole moment with the magnetic field of the electrons of the atom. The material used in this experiment was Co^{57} diffused into Pd as source, and metallic iron enriched with Fe^{57} as absorber. Since the peak of a Mössbauer line or the peaks of its hyperfine structure are fundamental constants expressed in velocity, they are ideally suited to measure velocities.

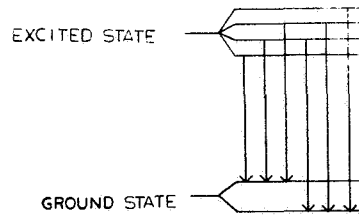
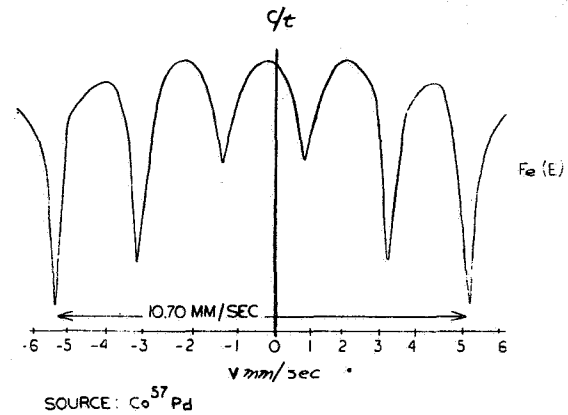


FIGURE 5. NUCLEAR ZEEMAN EFFECT

When using earlier methods to obtain vibration measurements, usually the amplitude or the acceleration was determined. Velocity variations were seldom considered. In utilizing the Mössbauer effect, however, velocity is measured. By restricting the vibrations examined in this investigation to steady state sinusoidal oscillations, it is possible to calculate with certainty (1) the displacement amplitude and acceleration from measuring the frequency, and (2) the velocity variations. However, it is also possible to measure nonharmonic oscillations.

Vibration investigations were conducted by using a loudspeaker and different piezoelectric transducers. The source is mounted on the vibrating object and the absorber is at rest. With this arrangement different cases can be investigated by using partial resonance, off resonance, and resonance conditions.

The partial resonance case makes use of the isomer shift in such a way that zero velocity corresponds to a certain count rate in the middle of the linear portion of the absorption curve (Fig. 6). Any positive or negative velocity will increase or decrease this count rate. Thus the velocity-time function will be transferred into a countrate-time function.

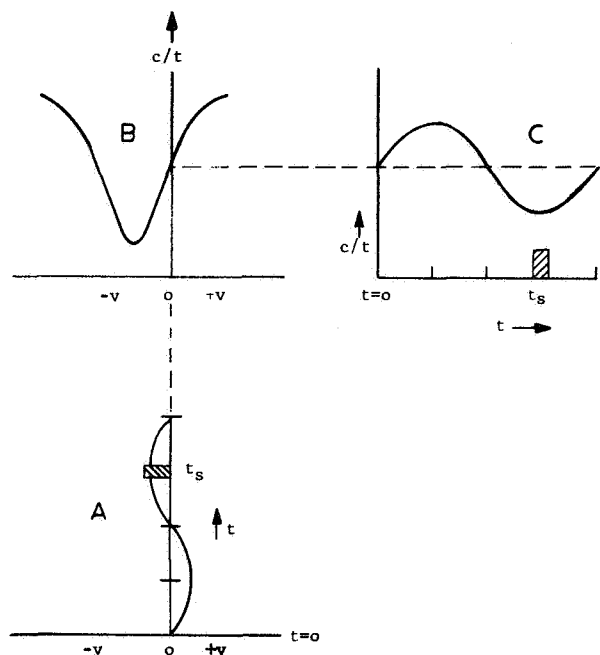


FIGURE 6. DIAGRAM OF THE PARTIAL RESONANCE CASE TRANSFER FUNCTION

An electronic device triggers the counter for an adjustable fraction of an oscillation period to permit repeated sampling within a small increment (Fig. 7). After enough counts have been collected for statistical accuracy, the gate is shifted by delaying the trigger pulse which opens the gate, and the next portion of the curve is counted. Finally point for point samples of a period have been collected. Corrections for the influence of gate length and nonlinearity of the characteristics are provided.

Figure 8 depicts amplitude measurements of a piezoelectric shaker. The upper portion shows the sinusoidal fluctuations of the countrate as collected point for point for one period, and by knowing the countrate-velocity relationship, the velocity curve on the bottom has been found. The peak amplitude is derived by the relation: velocity = amplitude times

angular frequency, which in this special case is 125 Å for 2 kHz at 35 V driving voltage. At higher frequencies even lower amplitudes can be measured, for example down to 3.5 Å at 10 kHz (Fig. 9).

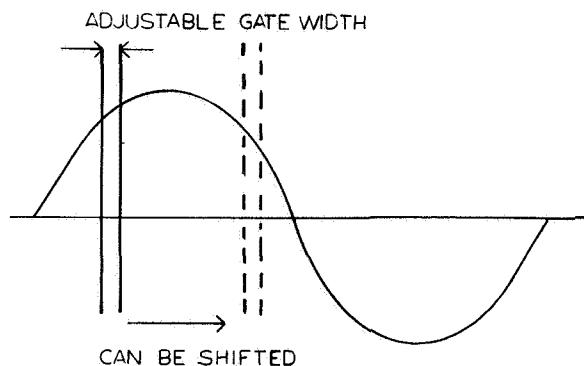


FIGURE 7. ELECTRONIC SAMPLING

The useful range of the partial resonance case is shown in Figure 10. This is a double logarithmic plot of velocity versus frequency for various values of acceleration and peak displacement. The lower frequency limit is arbitrarily set at the lower limit of the audio spectrum, the upper frequency limit is imposed by the experimental apparatus used. However, with an improved apparatus that is to be delivered soon, the limit of the technique will exceed 100 kHz.

Another method which is particularly of interest to vibration calibrations is the off resonance case. It deals with source and absorber combinations that are essentially out of resonance at zero velocity, but are tuned to resonance by an introduced relative velocity. These conditions can be obtained with material displaying quadrupole splitting or the nuclear Zeeman effect.

The basic idea of this method is that the calibration relies only on the position of the absorption lines of the hyperfine structure of various Mössbauer absorbers. The gating and sampling technique is similar to that of the off resonance case. Figure 11 illustrates the transfer function of this technique. The sinusoidal oscillation has a larger amplitude and exceeds the line of continuity in the spectral curve, which in this case represents the inner lines of metallic Fe⁵⁷. The remaining lines of this Zeeman splitted display were omitted to simplify the illustration. The outcome does not resemble the original sinewave,

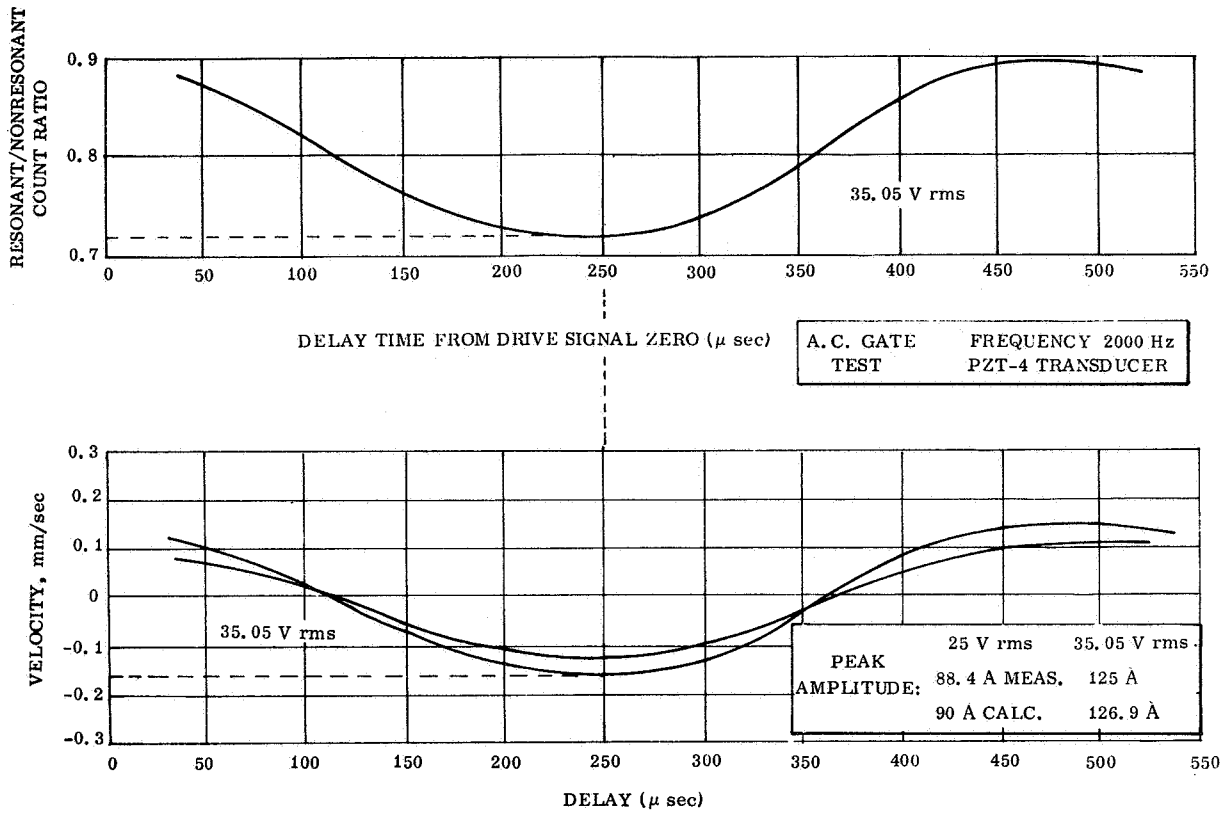


FIGURE 8. AMPLITUDE MEASUREMENTS OF A PIEZOELECTRIC SHAKER

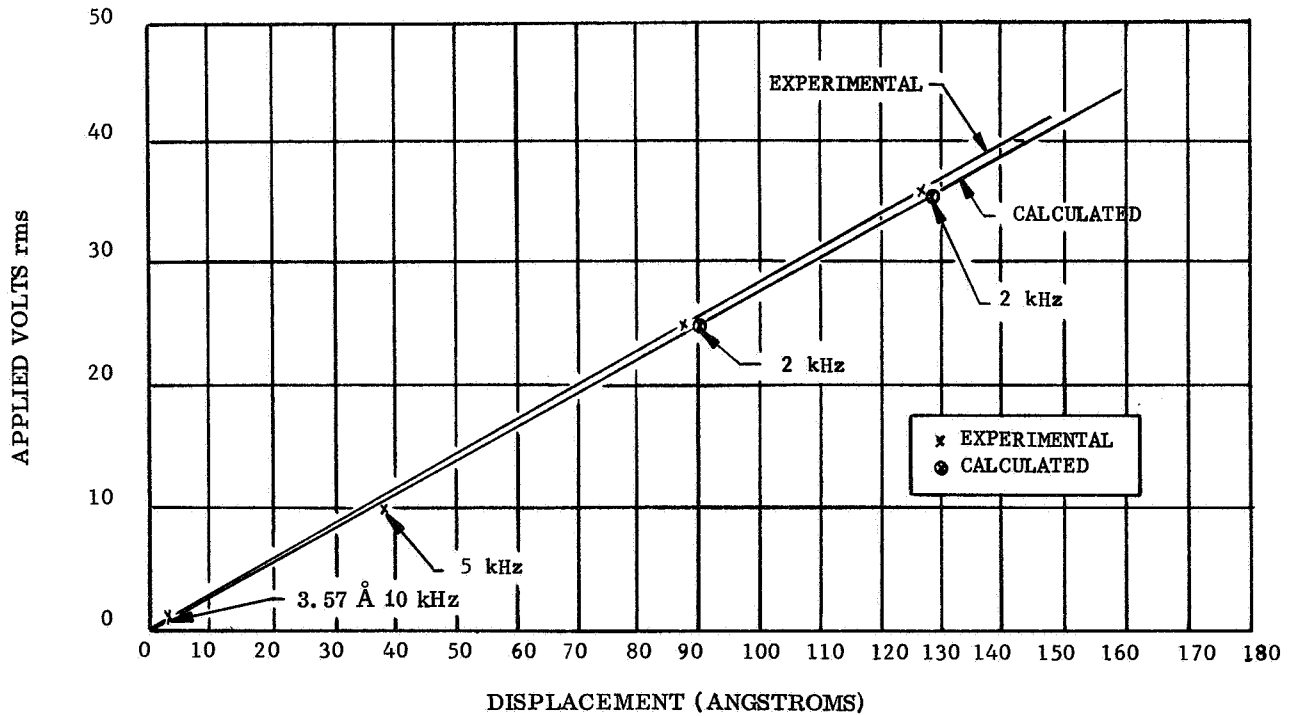


FIGURE 9. COMPARISON OF EXPERIMENTAL AND CALCULATED PEAK DISPLACEMENTS OF A PIEZOELECTRIC TRANSDUCER

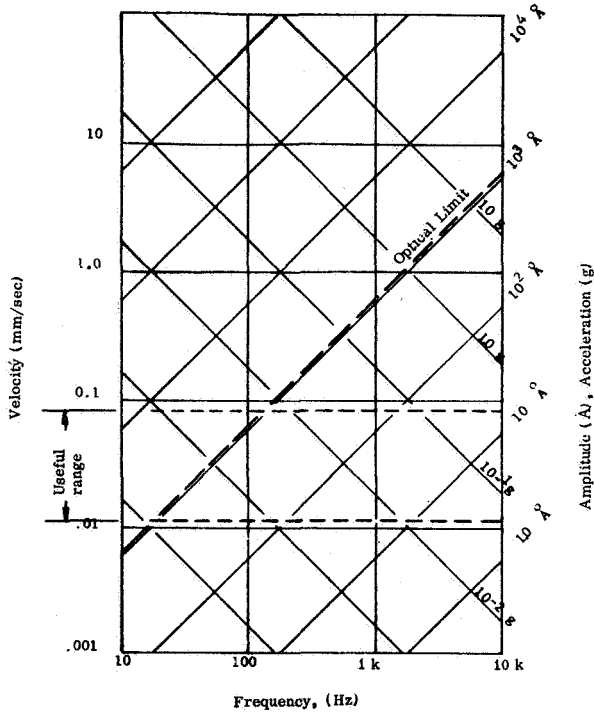


FIGURE 10. USEFUL RANGE OF PARTIAL RESONANCE CASE

but the extrema correspond to the extrema in the original curve, and furthermore, the discontinuities correspond to the spectral lines in the absorber spectrum. This permits a calibration based on fundamental constants as they are displayed in the Mössbauer spectrum. All one has to do is to set the electronic gating device to a positive or negative velocity maximum, which is determined by wave tracing as in the partial resonance case, and regulate the driving voltage of the oscillator until a minimum in the counting rate is reached. At this point the maximum velocity of the transducer is equal to the velocity associated with the spectral line of the absorber. If the frequency of the harmonic motion is known, the displacement amplitude can be calculated. Using different spectral lines of the hyperfine structure, or different absorbers, a variety of calibration points can be obtained.

Figure 12 shows the calibration curve of a small loudspeaker with unknown characteristics. The points delivered by isomer shift, quadrupole split, and Zeeman effect are marked. The peak amplitude was calculated from the frequency and the peak velocity. For 8 kHz the calibration factor is 56.4 Å per volt rms. This is just to demonstrate the simple calibration technique for small amplitude electromagnetic, ferroelectric, and piezoelectric transducers.

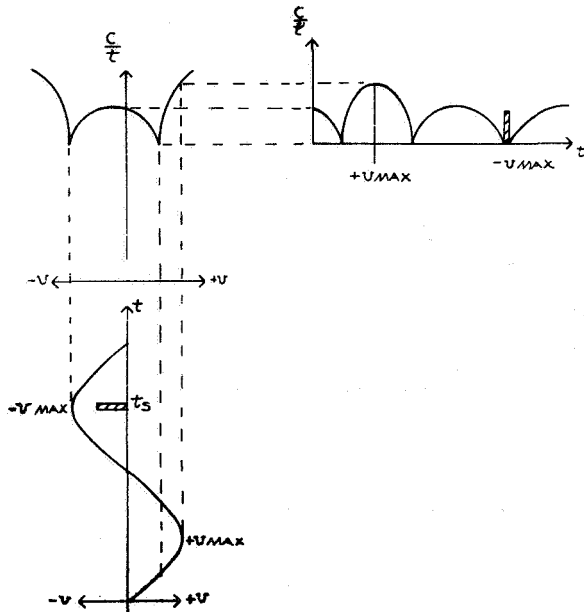


FIGURE 11. MULTIPLE POINT CALIBRATION TECHNIQUE TRANSFER FUNCTION

The useful range of this multiple point calibration technique is shown in Figure 13. This plot of velocity versus frequency is in the same scale as the similar graph describing the partial resonance case; however, here the useful range is broader and shifted to higher velocities. The frequency range of the new apparatus will exceed 100 kHz.

A third method that makes use of the Mössbauer technology for vibration measurements and calibration is the resonance case, which pertains to source-absorber combinations having unsplit lines and being resonant at zero velocity. The perfect resonance is disturbed if the source is allowed to vibrate, and the measured count rate will increase with increasing velocity.

While the resonance curves used in the previous cases were based on constant velocities, the resonance curve discussed now is derived by using sinusoidal velocities and has a different shape. Mathematically it is a function of the counts per unit time on average count rate N_0 , depending on the off resonance count rate N_0 , the peak velocity δ_1 , the full line width at half maximum Γ , and the absorption

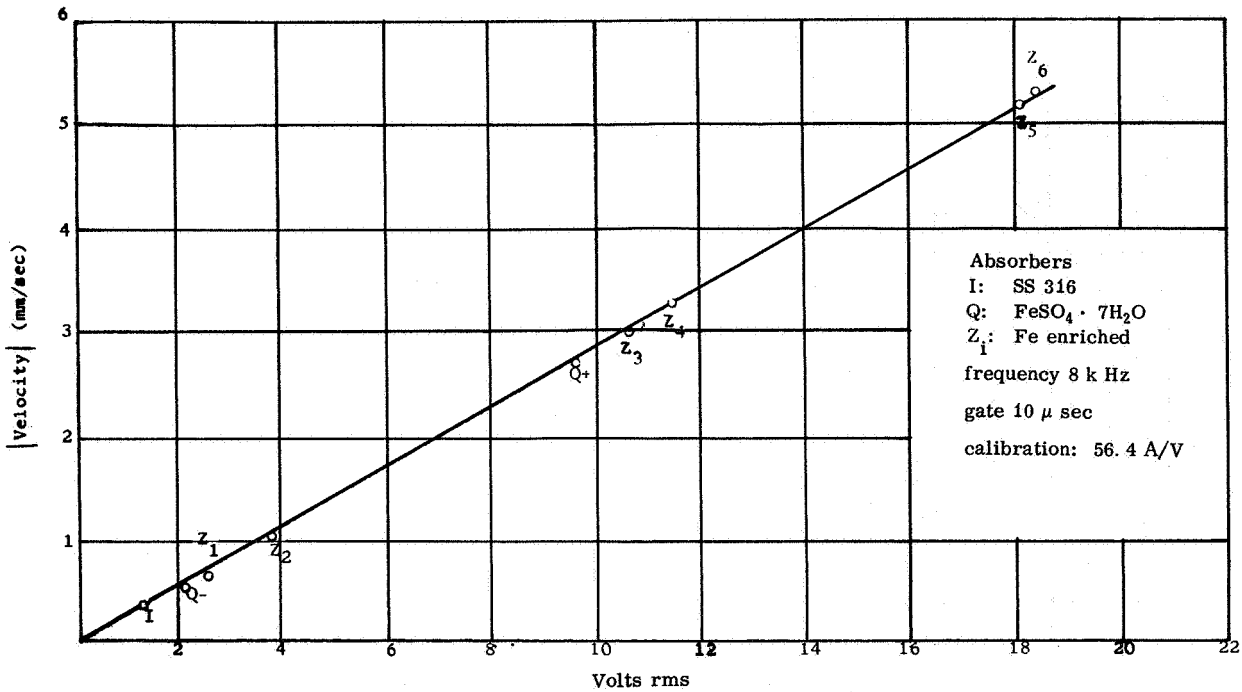


FIGURE 12. LOUDSPEAKER CALIBRATION BY RESONANCE
ABSORPTION LINE POSITION

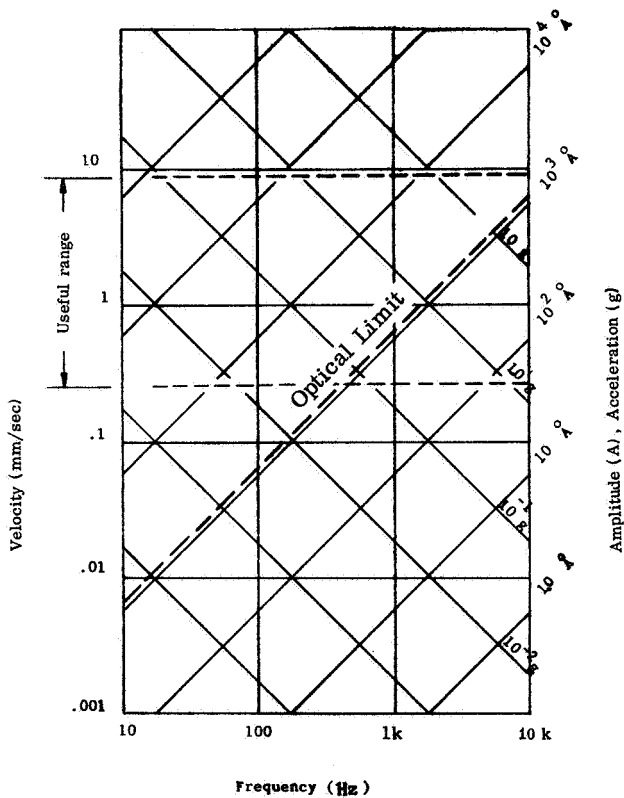


FIGURE 13. USEFUL RANGE OF THE MULTIPLE POINT CALIBRATION TECHNIQUE

fraction A, as given by

$$\frac{c}{t} = N_0 \frac{\delta_1^2 + 2\Gamma^2 A}{\delta_1^2 + 2\Gamma^2} \quad (1)$$

Figure 14 represents such an absorption curve. The difference at high velocities between the theoretical and the experimental values is caused by some simplified assumptions in the derivation of the equation. The lower curve was derived by introducing experimentally determined values for the constants Γ and A.

Both curves agree perfectly up to 0.4 mm/sec velocity. The lower curve is very well suited to calibrate piezoelectric transducers at low velocities. Two transducers were calibrated with this resonance technique. Data in Figure 15 were obtained with the source mounted on a loudspeaker. The driving frequency was 8 kHz. Displacements in the range of 10 to 100 Å could be measured. Figure 16 shows the calibration curve of a piezoelectric transducer excited by a 40 kHz signal. It was possible to measure displacements of a few angstroms.

Figure 17 shows the useful range of the resonance case calibration method. It can be seen that at high frequencies even fractions of an angstrom can be measured and respectively calibrated.

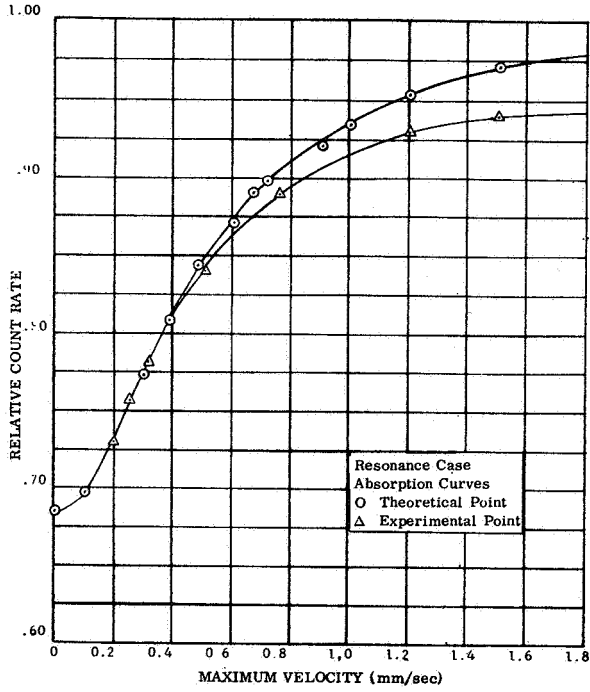


FIGURE 14. RESONANCE CASE ABSORPTION CURVES

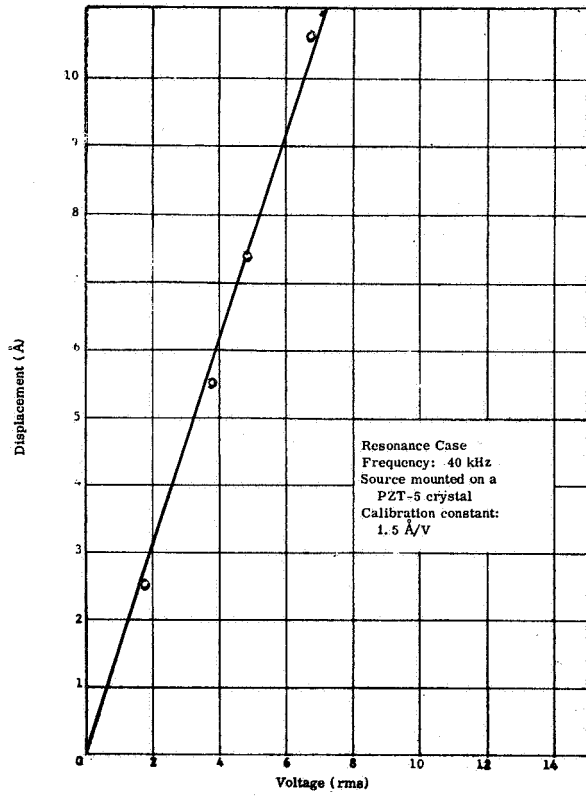


FIGURE 16. SOURCE MOUNTED ON PZT-5 CRYSTAL

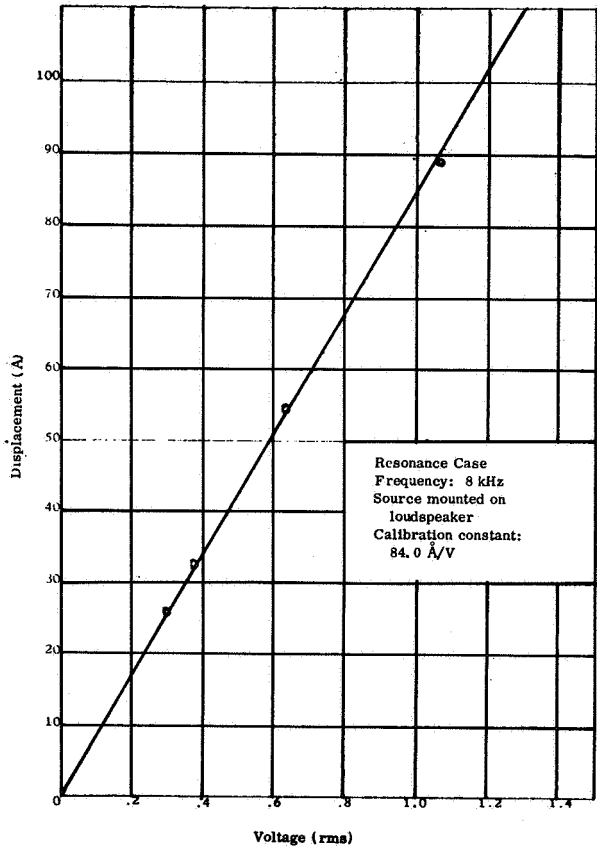


FIGURE 15. SOURCE MOUNTED ON LOUDSPEAKER

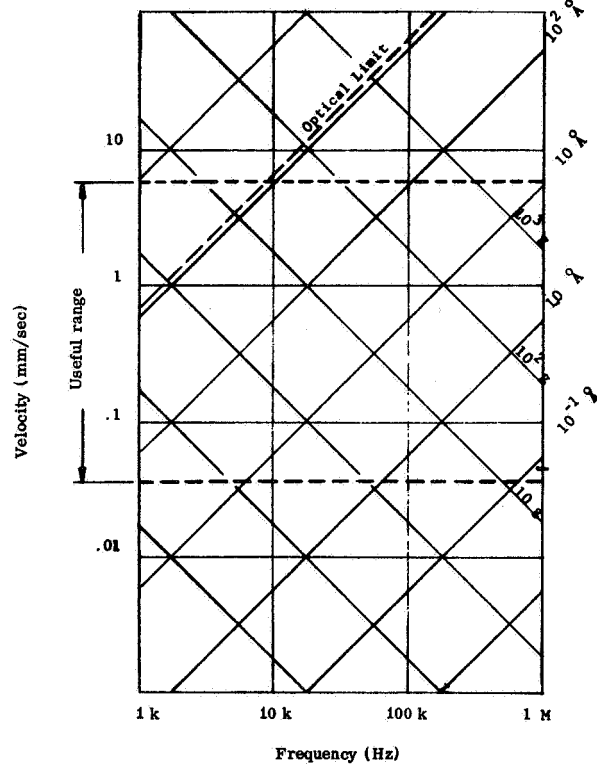


FIGURE 17. USEFUL RANGE OF THE RESONANCE CASE

This method has virtually no frequency limitation as long as the waveform is perfectly sinusoidal and the velocity falls within the useable range.

In the overall range the counting time required per point will be about three minutes and it will still be possible to keep the errors in peak velocity at 2% or less.

The development of these measuring and calibration methods was done at Rocketdyne. The contract requires the delivery of a laboratory calibrator (Fig. 18) and a transfer standard.

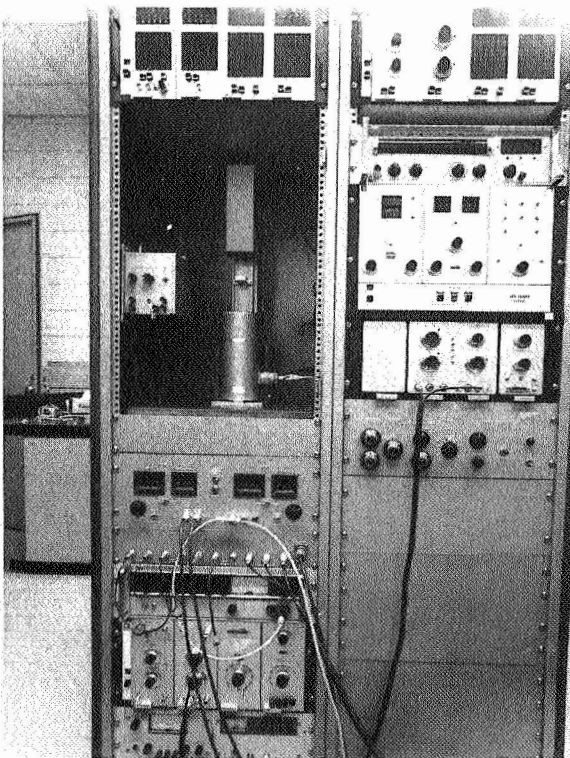


FIGURE 18. MÖSSBAUER EFFECT VIBRATION CALIBRATOR

The great advantage of the Mössbauer-type vibration calibrator is that it is based directly on an absolute standard, namely a Mössbauer line, which is a natural constant. However, the calibrations with

these methods have a general disadvantage: they are very time consuming and therefore are not likely to be used for routine calibrations where multiple data points in a short time are required. For this purpose optical methods are faster. In recent years optical methods have become known, and with these methods it will become possible to sense vibration amplitudes in the order of a few angstroms. However, although these methods are based on reasonable assumptions, they should be cross checked with an absolute method. This can be done with the absolute Mössbauer method.

LASER INTERFEROMETRY

Conventional interferometric methods are used to measure minimum vibration amplitudes in the order of one tenth of a wavelength only, which is not sufficient for our needs. Therefore, we initiated a contract with the National Bureau of Standards (NBS) to extend the optical measuring range at least two orders of magnitude below the conventional interferometric range. The method used to accomplish this measurement is especially suitable for calibration because it makes use of the monochromaticity, coherence, and intensity of laser light in an optical interferometer.

In the following, a short sketch will be given of the application of the laser interferometer in conducting vibration measurements and calibrations. If an interference pattern is formed by combination of two coherent beams of light in an interferometer, the current from the photocell receiving light from a small area is given by

$$I = A + B \cos k \delta, \quad k = \frac{2\pi}{\lambda} \quad (2)$$

where

$A, b \dots$ constants related to the intensity of the two light beams

$\delta \dots$ optical path difference between the two interfering rays

$\lambda \dots$ wavelength of the incident light.

This cos function of the photocurrent has nothing to do with an oscillating motion; it is obtained with stationary mirrors and represents the influence of the wavelength of the light and its phase as a result of differences in the optical pathlength.

Now, if one mirror vibrates sinusoidally, the difference in the optical pathlength δ changes sinusoidally and the current from the photodetector is given by

$$I = A + B \cos(k\delta + 2\xi \cos \omega t) \quad (3)$$

where

ξ ... amplitude of vibration

ω ... $2\pi f$, the angular frequency of the vibration.

The optical path difference δ may drift with changes in the dimension of the structure supporting the reflectors and can be adjusted by a dc bias applied to the shaker.

This expression for the photocurrent can be expanded in a Fourier series. The coefficients are expressed as Bessel functions with the argument ($2k\xi$).

$$\begin{aligned} I = A + B \cos k\delta & \left[J_0(2k\xi) - 2J_2(2k\xi) \cos 2\omega t \right. \\ & \left. + 2J_4(2k\xi) \cos 4\omega t \dots \right] \\ - B \sin k\delta & \left[2J_1(2k\xi) \cos \omega t - 2J_3(2k\xi) \cos 3\omega t \right. \\ & \left. + 2J_5(2k\xi) \cos 5\omega t \dots \right] \end{aligned} \quad (4)$$

where J_n is the Bessel function of the first kind and n th order. The separate terms of the Fourier series can be isolated by band pass filters. A filter set for the vibration frequency gives $C_1 \sin k\delta \cdot J_1(2k\xi)$, and a filter set for the second harmonic of the vibration gives $C_2 \cos k\delta \cdot J_2(2k\xi)$.

The constants C_1 and C_2 contain the insertion loss of a filter and also the constant B from the equations for the photocurrent.

The distance, δ , can be adjusted so that the ratio of the sin and cos factors is a known value, in particular, unity. Then the ratio of the output voltages of the second harmonic to the fundamental is

$$R_{21} = \frac{C_2}{C_1} \cdot \frac{J_2(2k\xi)}{J_1(2k\xi)} \quad (5)$$

If the series expansion of the Bessel functions is used, the ratio is

$$R_{21} = \frac{C_2}{C_1} \frac{\pi\xi}{\lambda} \left(1 + \frac{2\pi^2\xi}{3\lambda^2} + \frac{2\pi^4\xi^4}{3\lambda^4} + \frac{32\pi^6\xi^6}{45\lambda^6} + \dots \right) \quad (6)$$

This series converges for amplitudes less than the first zero of J_1 which is about 1920 Å. The convergence for larger values has not been investigated, but this is of no concern because larger values of amplitude can be covered by conventional optical methods.

If the 6328 Å line of a He-Ne laser is used, the error in dropping all terms of the series after the first is less than 1% for vibration amplitudes less than 240 Å. If the first two terms are used, a cubic equation has to be solved and the error is less than 1% for amplitudes less than 700 Å. Similarly, when using three terms and a slightly more complicated computer program, one can solve the fifth degree equation and find that the measuring range goes up to 1900 Å within an accuracy of 1%. This provides a considerable overlap with presently used methods. However, for the experiments done to investigate the usefulness of the theory, only the first order equation

$$\xi = \frac{\lambda}{\pi} \frac{C_1}{C_2} R_{21} \quad (7)$$

was used. The experimental setup is sketched in Figure 19. An oscillator drives a shaker whose vibrations are sensed by the laser-type interferometer and transformed into current by the photomultiplier. The photocurrent is analyzed by tracking filters that are synchronized from the oscillator, and the amplitude ratio of the second harmonic to the fundamental is obtained. To overcome difficulties in the zero drift of the shaker, an automatic feed-back mechanism is considered, the principle of which has been proved to work in manual operation.

It is felt that the uncertainties in vibration calibrations using this method would be about 2%.

Some preliminary results are given in Figure 20. This is a double logarithmic plot taken over four decades of amplitudes at 2 kHz. The abscissa is the shaker voltage, which can be assumed to be linear with displacement. The ordinates of the lines with the slope of one are the accelerometer output and the fundamental component of the photocurrent $E_1(x)$. The ordinate of the line with the slope of two is the component of the photomultiplier current with the

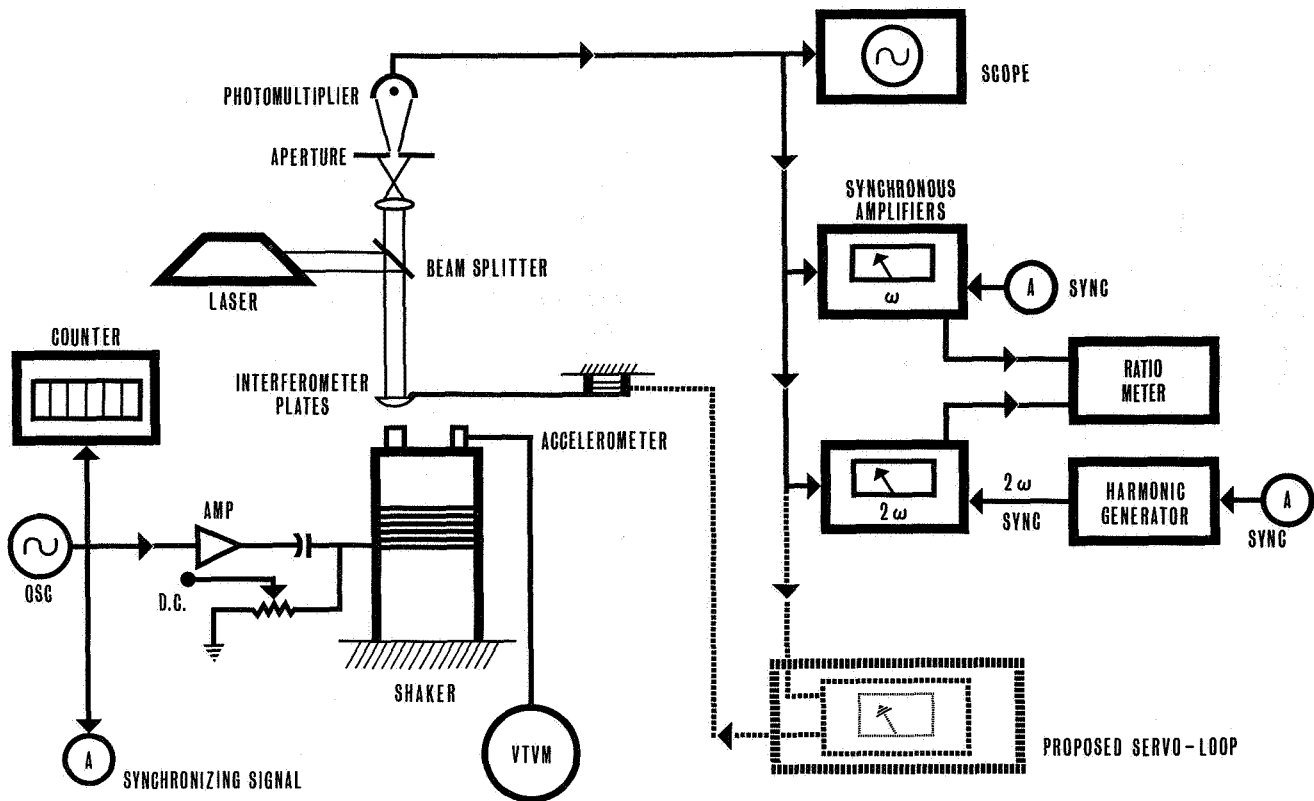


FIGURE 19. BLOCK DIAGRAM OF THE LASER INTERFEROMETRY SYSTEM

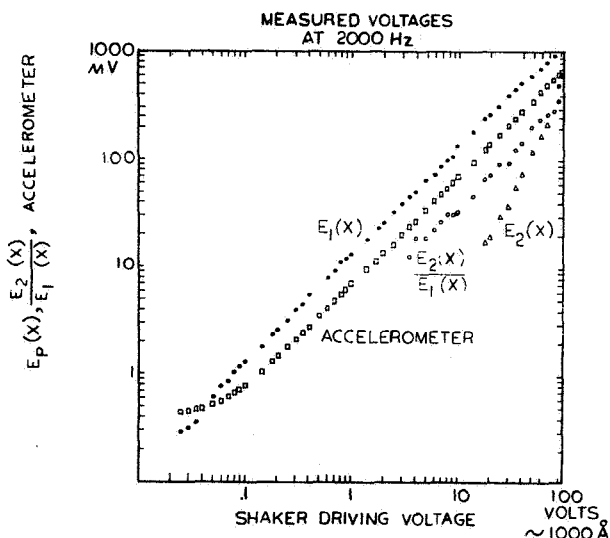


FIGURE 20. OUTPUT OF THE FUNDAMENTAL, OF THE FIRST HARMONIC, THEIR RATIO, AND OF THE MONITORING ACCELEROMETER VERSUS SHAKER DRIVING VOLTAGE

second harmonic $E_2(x)$. The ratio of the component of the photomultiplier signal at the second harmonic of the vibration frequency to the component at the fundamental vibration frequency $\frac{E_2(x)}{E_1(x)}$ is also shown with a slope of one. Figure 21 shows the result of similar measurements at 1 kHz. These data show linear relationship, which confirms that the experiment is in excellent agreement with the theory.

The signal of the second harmonic could be received to an amplitude of 10 Å. Below 10 Å it was lost in the noise in the photomultiplier and airborne sound in the room. Cooling with dry ice and a good sound insulation improved the measurements. Under favorable laboratory conditions 5 Å vibrations could be measured. The present main problem is the noise caused from improper electronics and hardware. Specifications for tracking filters have been written and two manufacturers responded positively. We expect that with improved filters the objective of the project, measurement and calibration of vibrations to within 1 Å amplitude at 100 kHz, can be reached.

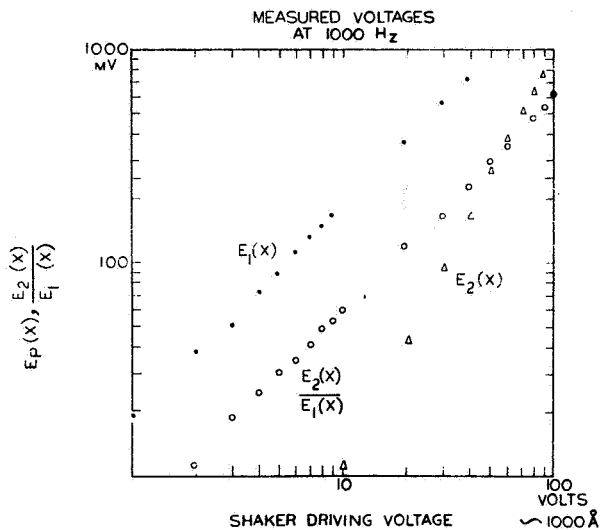


FIGURE 21. OUTPUT OF THE FUNDAMENTAL, OF THE FIRST HARMONIC, AND THEIR RATIO VERSUS SHAKER DRIVING VOLTAGE

Whether this method can be used for absolute calibrations depends on the linearity of the calibration factor for all lower amplitudes, once the system had been calibrated with a conventional method at 800 Å (in the first maximum of the first order Bessel Function). It is reasonable to assume that the calibration factor holds to 1 Å amplitude or even below because this method has the advantage that it requires only the ratio of two calibration factors to be linear over the range of amplitudes rather than the absolute value of either, and this linearity has been demonstrated in Figures 20 and 21.

On the other hand, the availability of the calibration method using the Mössbauer Effect gives for the first time an independent, nonoptical way of verifying the accuracy of the optical calibration method. The two methods provide cross-checks that guard against systematic errors in either calibration method. In fact, several organizations from government as well as from private industry requested information about this unique possibility of cross-checking the interferometer with an independent, nonoptical method.

The National Bureau of Standards is working on a method that provides vibration calibrations below 800 Å. This is accomplished with an interferometer in which one light path is extended by multiple reflections between a stationary and an oscillating mirror, thus increasing the sensitivity by the number of reflections. As depicted in Figure 22, light from a

He-Ne gas laser is divided by a beam splitter. The transmitted beam is reflected from a mirror on the shake table to an auxiliary, stationary mirror and back to the vibrating mirror a number of times, and then to a second beam splitter where part of it is combined with the reflected beam from the first beam splitter to form an interference pattern. The convenience of the method results from the intensity and collimation of the laser light. Each reflection produces a small red spot on the mirror so that the system can be aligned easily, and the number of reflections can be counted easily without ambiguity. The focusing lens is used to insure that the laser beam is as narrow as possible in the region of multiple reflections. It expands beyond that region. The optical attenuator is used to adjust the intensity of the light reflected from the first beam splitter to match the intensity of the light from the vibrating surface. The expander lens is used to set the fringe pattern to an optimum size and intensity for visual observation.

The folded beam interferometer is used to set the amplitude of vibration to a known value by the techniques of interference fringe disappearance. If the 6328 Å line of the He-Ne laser is used, the usual fringe disappearance would occur at 1211 Å. In the folded beam interferometer, disappearance occurs at 1211 Å divided by the number of reflections.

This method works fine, provided all surface elements are oscillating in phase. This has been checked by placing three accelerometers on the shaker surface and comparing their output voltages on the x and y plates of an oscilloscope. If all transducers are oscillating in phase, the display on the scope is a straight slant line. If they are out-of-phase, the scope shows an ellipse.

It has been found that up to 30 kHz the shaker is oscillating in phase all over its surface. At higher frequencies this is not guaranteed any more; however, for calibration purposes, certain frequencies where there is no uniformity in phase have to be avoided.

In a laboratory setup ten reflections could be achieved, which means that with the He-Ne laser vibration amplitudes down to 120 Å could be detected.

The contract with the NBS contains provisions for the development of shakers covering a frequency range up to 100 kHz, but this is not a subject of this paper.

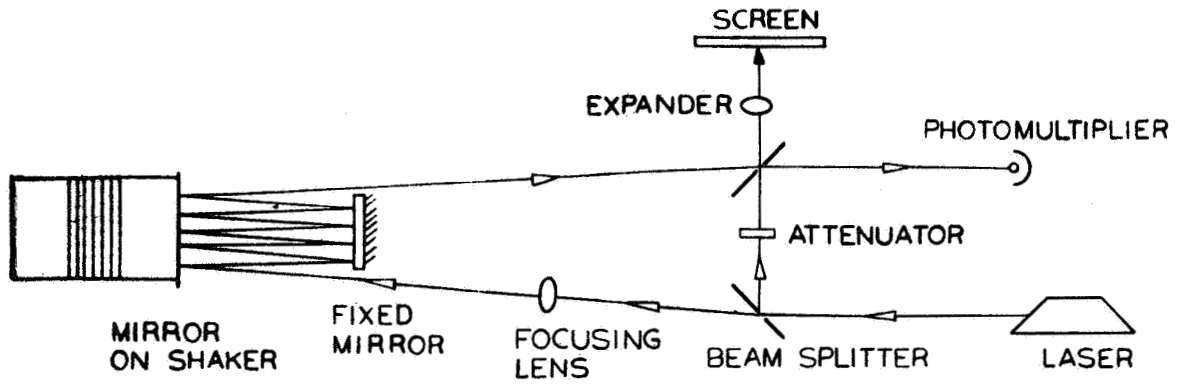
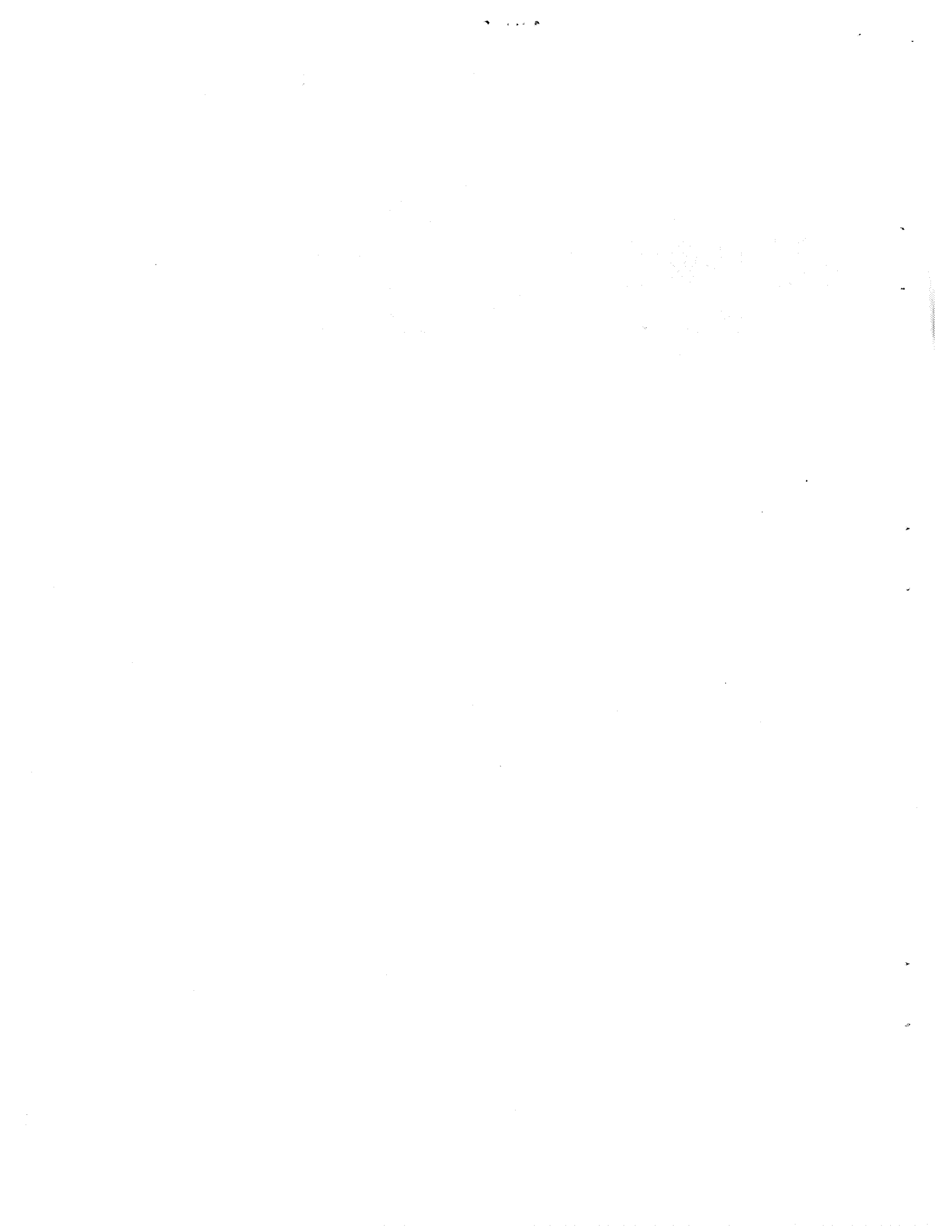


FIGURE 22. MULTIPLE BEAM REFLECTION INTERFEROMETER



PARACTOR, A NEW TOOL FOR ACCURATE DC AMPLIFICATION AND DIGITAL DATA TRANSMISSION

By

Thomas L. Greenwood

INTRODUCTION

Several years ago the Test Laboratory became interested in the development of an improved digital data acquisition system in which the analog transducer output would be converted to digital form in the vicinity of the transducer. Transmitting the data in digital form will reduce the probability of error caused when long cable circuits carry analog signals. Contract NAS8-5439 was awarded to Trans-Sonics, Inc., to develop such a system using magnetic amplifier techniques in the comparison circuit of a successive-approximation analog-to-digital converter.

The Parametron, invented by Goto of Tokyo University and used extensively in Japanese computers as a logic element, seemed suited to this application. It has the property of producing oscillations with the phase depending on polarity of magnetic flux in the input coil, and can be produced in small physical dimensions approximating the size of a cable connector.

PARACTOR RESEARCH AND DEVELOPMENT

Investigation of the Parametron device by Trans-Sonics, Inc., engineers showed that significant improvements could be made in its operation. The improved Parametron, a form of second harmonic modulator, was called the Paractor, for "parametric reactor." It was driven by a continuous wave ac, and developed a large ac output in the form of a self-oscillation, the phase of which was under the control of the dc input signal. Only two phases could be generated, 0 and π radians, and these signals could be used as commands to control the logic steps in the successive-approximation technique for analog-to-digital conversion. The circuit was the super-regenerative type in that the phase of the output signal could not be changed without first stopping the oscillations.

Further improvement indicated that this Paractor, while exhibiting very high gain, had one property that

was extremely undesirable in the case of the planned application. This property was that the Paractor "remembered" large input signals. Any overload of the control winding caused a zero shift in the Paractor, which was equivalent to a direct current in the input winding.

The Paractor circuit was modified to provide pulse excitation instead of sine wave excitation, and is now known as the Pulsed Paractor. Its operation may be described as follows: The coil that carries the control or input signal as well as the output pulses is referred to as the flux coil (Figs. 1 and 2).

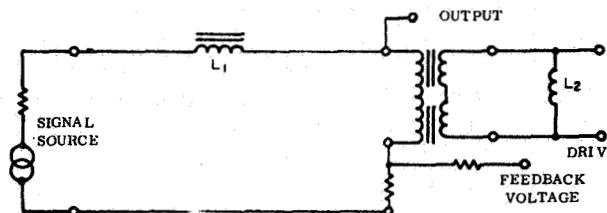


FIGURE 1. PULSED PARACTOR

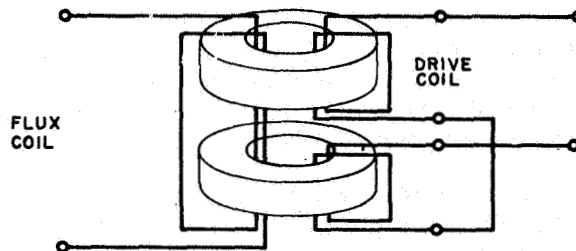


FIGURE 2. PARACTOR MAGNETIC CIRCUIT

The two coils through which the drive pulse is applied are called drive coils, and the circuit that includes the drive coils and the apparatus driving the coils is referred to as the drive circuit. The function of the drive coils is merely to establish the permeability of the cores around which the flux coil is wound. To prevent drive currents from being induced in the flux

coil, the magnetic material is divided into two cores, each of which carries a drive coil. The drive coils are connected so that the drive flux induced in each of the two cores is in opposite directions. For example the upper core might have flux induced in the clockwise direction while the lower core might have flux induced in the counterclockwise direction. If these fluxes are identical, no voltage would be induced in the flux coil that threads both cores (Fig. 2).

Immediately before the drive pulse is applied, the cores are in a state of high permeability. Any signal current flowing in the flux coil will result in a relatively high flux being induced in the two cores inside the flux coil. This flux is caused by the control signal operating on the high permeability of the cores. The drive pulses are of sufficient amplitude to drive the cores into saturation. As the cores saturate, the instantaneous permeability of the iron decreases and approaches zero as a limit. As the permeability approaches zero the flux induced by the control signal must disappear since the permeability is too low to support the flux. As the flux disappears, a voltage is induced in the flux coil as a result of the rate of change of flux. This voltage is the output signal, the phase or polarity of which depends on the polarity of the direct current in the input coil. Rapid saturation is necessary to obtain a large output. This is accomplished by driving the cores with a large current pulse having a low duty cycle.

The output pulse is prevented from flowing back into the dc source circuit by the inductor L_1 . Resetting the cores to a zero magnetic condition is accomplished by the "kickback" from the inductor L_2 after the drive pulse has decayed to zero. The inductance value is chosen so that the "kickback" is strong enough to reduce the magnetism of the saturated cores to zero between each drive pulse. This eliminates the undesirable "memory" effect that was encountered in the early prototype models.

The magnetic modulators, or Pulse Paractors, designed and constructed on Contract NAS8-5439, have gains as high as 60 dB, and production quality control may guarantee gains as high as 55 dB. Signals in the order of 10-15 W in the input circuit have been amplified to a useful level.

MULTICHANNEL DIGITAL DATA ACQUISITION SYSTEM

DESIGN OF 120 CHANNEL SYSTEM

The goal of the development contract was a multichannel digital data acquisition system, and after the

Pulsed Paractor was developed to a point where its usefulness was demonstrated, specifications were written for a 120 channel system with magnetic tape recording.

The original concept of an improved system was to accomplish the analog-to-digital conversion as near to the transducer output as possible. The digital data could then be transmitted to any distance without degradation. Present analog-to-digital conversion systems, which include several hundred feet of wire conducting the analog signals to the conversion equipment, suffer degradation of the analog signal as a result of noise and other disturbances in the wire. The system concept provided for the conversion function to be accomplished in a circuit that has the comparator within a few inches of the transducer output terminals. The comparator-logic loop could be as much as a few hundred feet long without affecting the operation, as the logic signals are in digital form and would not be degraded by the wire link circuit. Thus, the comparator could be a small size suitable for mounting in the same environment as the transducer, and the logic circuit could be some distance away in a sheltered location.

DEVELOPMENT OF COMPARATOR CIRCUIT

Development of the system proceeded along these lines, and a prototype with a signal channel was successfully operated. However, it was realized that serious problems in the transmission of logic signals to the comparator would have to be solved if a system for a large number of channels could be designed. This circuit is shown in Figure 3. The bandwidths required might be in the order of 1 MHz. It was decided to try another approach. Figure 4 shows a circuit in which the feedback "balancing" voltage from the logic circuits is transmitted as a narrow band signal. However, this still required that the Paractor pulse output be transmitted over a wide band circuit. Further improvement in operation was obtained by using the circuit in Figure 5. The Paractor pulse output is integrated and sent to the logic equipment as a narrow band signal. This signal controls the decision-making function in the logic circuits, and the logic output signals are sent as narrow band voltage steps to the comparator input circuit to provide a potentiometric measurement of the input signal.

This comparator circuit provides all the functions and advantages as the original circuit concept. It transfers a high level replica of the input signal, through a tight feedback loop, to a convenient point for analog-to-digital conversion.

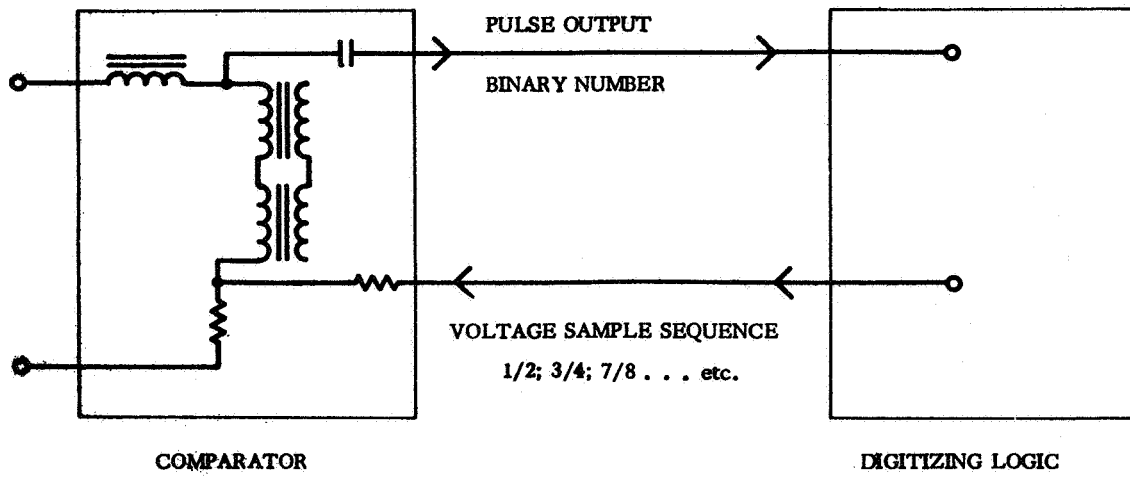


FIGURE 3. INITIAL INPUT CONFIGURATION

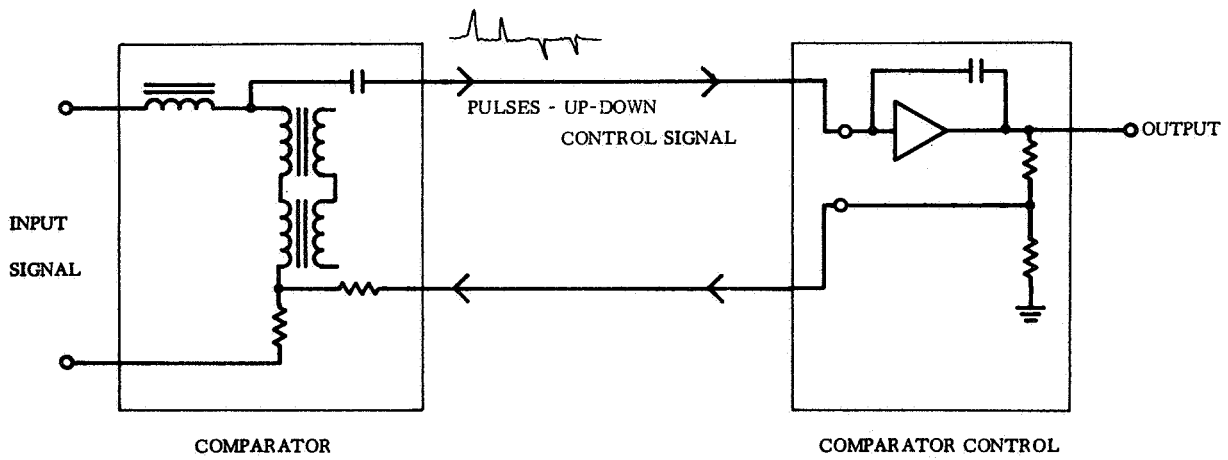


FIGURE 4. IMPROVED CIRCUIT

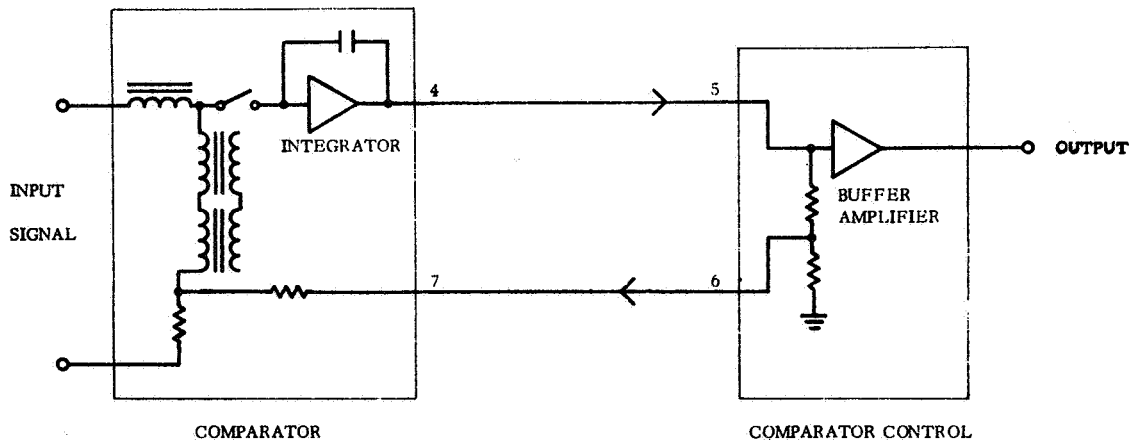


FIGURE 5. FINAL CONFIGURATION

DESCRIPTION OF THE SYSTEM

A system was designed and constructed for 120 channels, using the comparator circuit described above, each channel being sampled 20 times per second with a resolution of 1 part in 2000. Input

signals are ± 5 V fixed fullscale range, and a variable fullscale range from 10 to 50 mV. The equipment arrangement is shown in Figure 6 together with relative distances between the components of the system. Figure 7 shows a block diagram of the system.

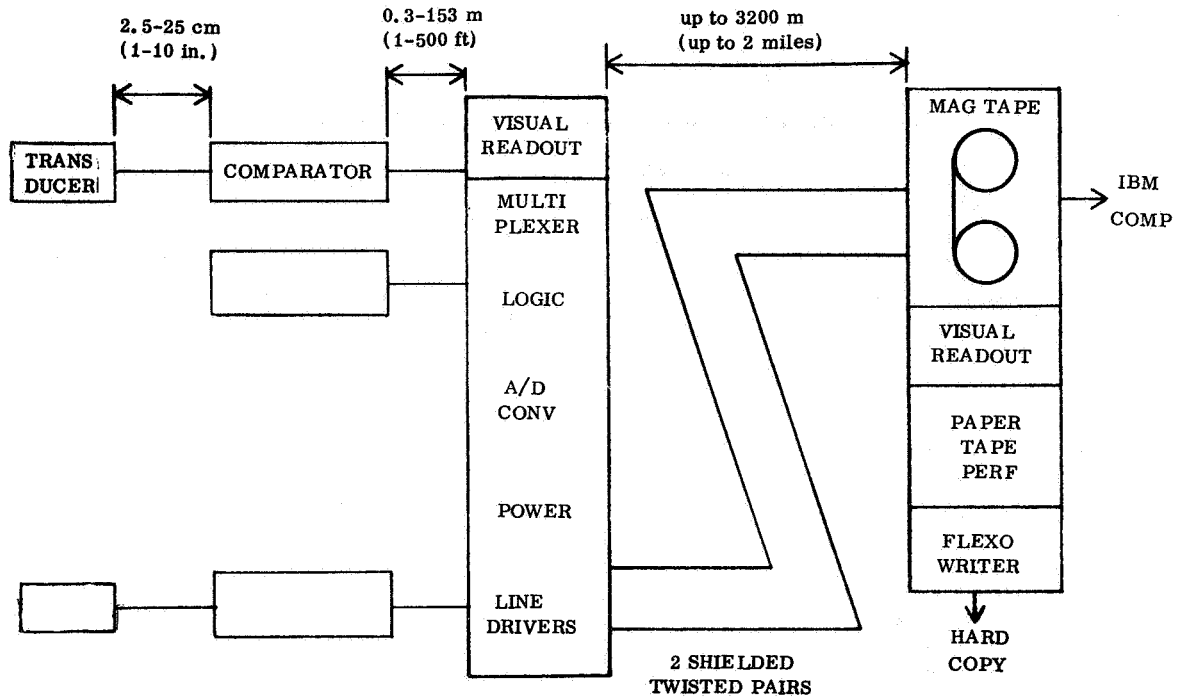


FIGURE 6. ARRANGEMENT OF COMPONENTS

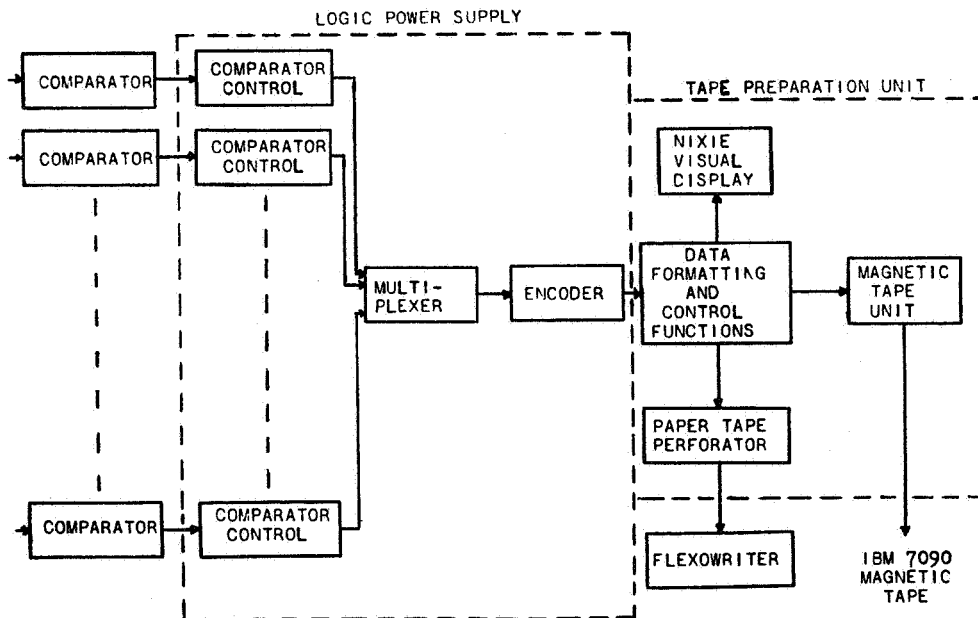


FIGURE 7. SYSTEM BLOCK DIAGRAM

The comparator unit includes a Pulsed Paractor, a pulse oscillator for driving the Paractor coils, an integrating amplifier, and resistance network for the feedback voltage providing the potentiometric measurement. This is encased in an environment-proof cylindrical enclosure of 3.3 cm (1.3 in.) diameter and 20.3 cm (8 in.) length. Cable connectors are provided at each end.

Logic control, power supplies, and visual digital monitors are provided in equipment racks suitable for mounting in the instrument room of a test stand, or other sheltered place. The digital signals are transmitted over two shielded twisted pairs to the recorder, which may be as far away as 2 miles. At the recording location, which could be a blockhouse, is the magnetic tape recorder, visual digital monitor, paper tape perforator and Flexowriter for printout. The magnetic tape recorder is the incremental digital type, which uses tape only when recording digital pulses, and produces IBM compatible tape recordings. The system has been checked out at Marshall Space Flight Center and has been put to use gathering data in Test Laboratory operations.

ADDITIONAL APPLICATIONS

Besides attaining the goal of the contract, the development of the precision comparator circuit gave promise of other applications in the instrumentation field. Trans-Sonics, Inc., packaged the new comparator circuit in a single enclosure as a "Precision dc Amplifier" using the circuit shown in Figure 8. This is essentially an electronic-servo-balanced potentiometric measuring system, similar in technique to a servo-balance strip-chart recorder. The amplifier is designed for input signals in the millivolt ranges. The output is an optional 5 or 10 V. The bandwidth extends from 0 to 1 kHz. Provisions are made for use with various transducers, including resistance thermometers, strain gages, and thermocouples. A regulated power supply and bridge completion networks are provided for transducer bridge circuit requirements. Primary power supply requirement is 28 Vdc. Figure 9 shows the packaged amplifier.

The Paractor input coil, being usually a low resistance, lends itself to various low impedance circuits. For example, for strain measurement without strain gages on the metal skin of a structure like a missile, electrical connections would be attached at the corners of a square, with excitation current being

supplied to opposite corners, and the output reading would be taken from the other diagonal connections. This is essentially a low resistance bridge circuit. Any change in resistance of a portion of the skin, caused by strain, would change the resistance balance of the bridge circuit, and the output would be amplified by the Paractor amplifier. The advantage is that the Paractor provides its best amplification when the input circuit is a low resistance.

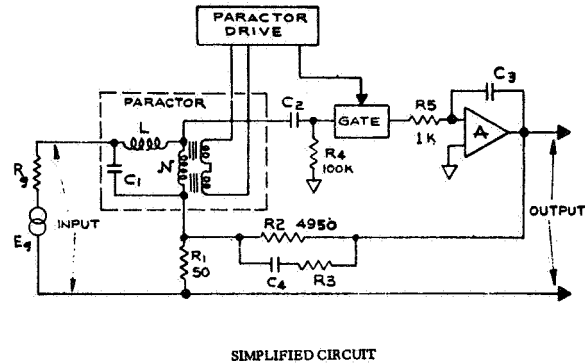


FIGURE 8. PRECISION AMPLIFIER USING PARACTOR

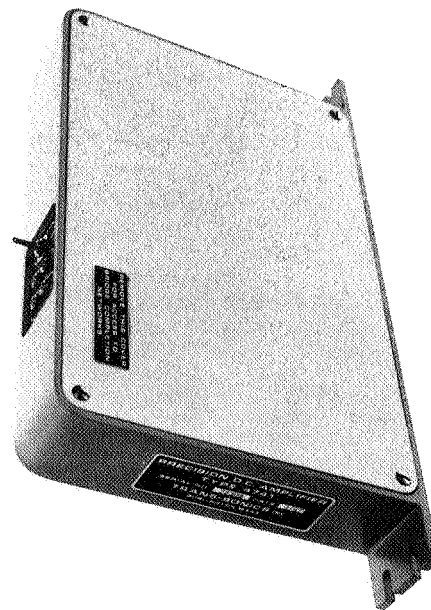


FIGURE 9. PRECISION DC AMPLIFIER

CONCLUSIONS

The goal of the development contract NAS8-5439 has been attained. A 120 channel digital data acquisition system has been developed and checked out satisfactorily, and is now used in Test Laboratory opera-

tions. A precision dc amplifier with improved characteristics has also been obtained by using techniques developed for the digital system. Its features of good stability under unfavorable environmental conditions, such as temperature extremes and vibration, have been demonstrated. This amplifier should prove useful in many instrumentation applications.

APPROVAL

RESEARCH ACHIEVEMENTS REVIEW
VOLUME II REPORT NO. 12

The information in these reports has been reviewed for security classification. Review of any information concerning Department of Defense or Atomic Energy Commission programs has been made by the MSFC Security Classification Officer. These reports, in their entirety, have been determined to be unclassified.

These reports have also been reviewed and approved for technical accuracy.



K. L. HEIMBURG
Director, Test Laboratory

UNITS OF MEASURE

In a prepared statement presented on August 5, 1965, to the U. S. House of Representatives Science and Astronautics Committee (chaired by George P. Miller of California), the position of the National Aeronautics and Space Administration on Units of Measure was stated by Dr. Alfred J. Eggers, Deputy Associate Administrator, Office of Advanced Research and Technology:

"In January of this year NASA directed that the international system of units should be considered the preferred system of units, and should be employed by the research centers as the primary system in all reports and publications of a technical nature, except where such use would reduce the usefulness of the report to the primary recipients. During the conversion period the use of customary units in parentheses following the SI units is permissible, but the parenthetical usage of conventional units will be discontinued as soon as it is judged that the normal users of the reports would not be particularly inconvenienced by the exclusive use of SI units."

The International System of Units (SI Units) has been adopted by the U. S. National Bureau of Standards (see NBS Technical News Bulletin, Vol. 48, No. 4, April 1964).

The International System of Units is defined in NASA SP-7012, "The International System of Units, Physical Constants, and Conversion Factors," which is available from the U. S. Government Printing Office, Washington, D. C. 20402.

SI Units are used preferentially in this series of research reports in accordance with NASA policy and following the practice of the National Bureau of Standards.

CALENDAR OF REVIEWS

FIRST SERIES (VOLUME I)

<u>REVIEW</u>	<u>DATE</u>	<u>RESEARCH AREA</u>	<u>REVIEW</u>	<u>DATE</u>	<u>RESEARCH AREA</u>
1	2/25/65	RADIATION PHYSICS	12	9/16/65	AERODYNAMICS
2	2/25/65	THERMOPHYSICS	13	9/30/65	INSTRUMENTATION
3	3/25/65	CRYOGENIC TECHNOLOGY	14	9/30/65	POWER SYSTEMS
* 4	3/25/65	CHEMICAL PROPULSION	15	10/28/65	GUIDANCE CONCEPTS
5	4/29/65	ELECTRONICS	16	10/28/65	ASTRODYNAMICS
6	4/29/65	CONTROL SYSTEMS	17	1/27/66	ADVANCED TRACKING SYSTEMS
7	5/27/65	MATERIALS	18	1/27/66	COMMUNICATIONS SYSTEMS
8	5/27/65	MANUFACTURING	19	1/6/66	STRUCTURES
9	6/24/65	GROUND TESTING	20	1/6/66	MATHEMATICS AND COMPUTATION
10	6/24/65	QUALITY ASSURANCE AND CHECKOUT	21	2/24/66	ADVANCED PROPULSION
11	9/16/65	TERRESTRIAL & SPACE ENVIRONMENT	22	2/24/66	LUNAR AND METEOROID PHYSICS

* Classified. Proceedings not published.

SECOND SERIES (VOLUME II)

<u>REVIEW</u>	<u>DATE</u>	<u>RESEARCH AREA</u>	<u>REVIEW</u>	<u>DATE</u>	<u>RESEARCH AREA</u>
1	3/31/66	RADIATION PHYSICS	7	3/30/67	CRYOGENIC TECHNOLOGY
2	3/31/66	THERMOPHYSICS	8*	5/25/67	COMPUTATION
3	5/26/66	ELECTRONICS	9	7/27/67	POWER SYSTEMS
4	7/28/66	MATERIALS	10	9/28/67	TERRESTRIAL AND SPACE ENVIRONMENT
5	9/29/66	QUALITY AND RELIABILITY ASSURANCE	11	11/30/67	MANUFACTURING
6	1/26/67	CHEMICAL PROPULSION	12	1/25/68	INSTRUMENTATION RESEARCH FOR GROUND TESTING

* Proceedings will be summarized only

Correspondence concerning the Research Achievements Review Series should be addressed to:
Chief, Research Program Office, R-EO-R, Marshall Space Flight Center, Alabama 35812